Physics – Uspekhi **65** (9) 920 – 951 (2022)

REVIEWS OF TOPICAL PROBLEMS PACS numbers: **03.30.+p**, **04.20.–q**, **06.20.–f**, **91.30.–f**, **03.75.–b**

Measuring global gravity-inertial effects with ring laser interferometers

V N Rudenko, S I Oreshkin, K V Rudenko

DOI: https://doi.org/10.3367/UFNe.2021.12.039128

Contents

Abstract. **We discuss advances achieved over the past 20 years in physical experiments on measuring the gravity-inertial background of Earth's surface associated with astrodynamical, geodynamical, and geophysical effects generated by Earth's internal gravity and thermodynamics and by its diurnal and orbital rotation. We discuss a unique instrument, a large-scale Sagnac ring laser interferometer, with a record high sensitivity to variations in the rotation rate and inclination of the laboratory reference frame, as well as to the rotational asymmetry of the optical refractive index of a medium, including a vacuum. These tools allow obtaining knowledge that is simultaneously valuable for elementary particle physics, quantum field theory, laser physics, astrometry, global geodynamics, and seismology. Applications may consist in an early forecast of global cataclysms such as earthquakes and progress in the metrology of angular measurements.**

V N Rudenko [(1, 2, *)], **S I Oreshkin** [(1)], **K V Rudenko** [(2)]
[(1)] Lomonosov Moscow State University,
Sternberg Astronomical Institute,
Universitetskii prosp. 13, 119992 Moscow, Russian Federation
[(2)] Lomonosov Moscow State University, Faculty of Physics,
Leninskie gory 1, str. 2, 119991 Moscow, Russian Federation
E-mail: [(*)] valentin.rudenko@gmail.com

Received 26 May 2021, revised 24 November 2021
Uspekhi Fizicheskikh Nauk **192** (9) 984 – 1018 (2022)
Translated by S Alekseev

Keywords: inertial sensors, Sagnac interferometer, measurements of Earth's rotation, toroidal modes, gravitational magnetism effect, dark matter particles, quantum measurements, matter wave interferometers, precision goniometers

1. Introduction

Gravitational measurements (experiments) on terrestrial and cosmic scales are currently an actively developing field of fundamental and applied science. The progress achieved in both theory and experiment over the past decades is clearly illustrated by accomplishments such as the detection of gravitational waves of an astrophysical nature, the discovery of stellar-mass black holes and supermassive black holes in galactic nuclei, advances in laser ranging of planets and spacecraft, detailed measurements of Earth's geoid by a system of geodetic satellites, the development of chronogeodesy with optical frequency standards, the creation of ballistic gravimeters based on cold atoms, and so on. Attention to gravitational experiments is obviously dictated by the modern idea of gravity as a phenomenon underlying the universe. The main research tools and methods are optical measuring instruments, methods for precision radio interferometry, and optical and atomic interferometry.

Instruments that measure gravitational forces (accelerations) cannot distinguish them from inertial forces (which is a statement of the equivalence principle). The surface gravity acceleration **g** is a vector combination of Newtonian attrac-

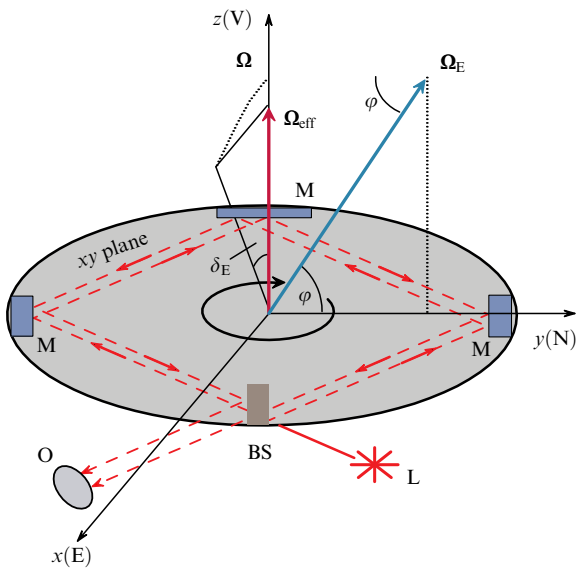

Figure 1. (Color online.) SG ring interferometer on Earth's surface. The effective angular velocity is $\Omega_{\rm eff} = \Omega_{\rm E} \sin(\varphi + \delta_{\rm N}) \cos\delta_{\rm E}$, where $\Omega_{\rm E}$ is the angular velocity of Earth, $\delta_{\rm N}$ and $\delta_{\rm E}$ are the angles of deviation to the north and east (at the position in the figure, $\delta_{\rm N} = 0$), and φ is the SG location latitude; M — mirror, BS — beam splitter, O — detector, L — laser.

tion $\mathbf{F}_{\rm G}$ and the centrifugal force of inertia due to Earth's rotation, $\mathbf{F}_{\rm I}$. It is impossible to separate just the Newtonian force by ground-based experiments. But it is possible to build an inertial instrument measuring the angular velocity $\mathbf{\Omega}_{\rm E}$ of Earth's rotation. This is an extremely important issue in astronomy: knowledge about the value of the modulus $|\mathbf{\Omega}_{\rm E}|$ and angular variations $(\mathbf{\Omega}_{\rm E}/|\mathbf{\Omega}_{\rm E}|)$ of Earth's axis is important for precision astrometry, space navigation, and fundamental astrophysical measurements.

It is known that the angular velocity of a rotating platform can, in principle, be measured with a ring optical interferometer using the Sagnac effect [1, 2] (for other applications, see, e.g., [3]). A ring optical cavity mounted on a rotating solid platform rotates together with it about the central symmetry axis normal to its plane with an angular velocity $\mathbf{\Omega}$ (in Fig. 1, $\mathbf{\Omega} = \mathbf{\Omega}_{\rm eff}$). The cavity modes for waves propagating along and against the direction of rotation then split: a shift in their resonance frequencies occurs. The addition of these waves gives an interference pattern along the circumference of the ring, which changes as the rotation speed changes. For a frequency shift of the modes $\delta f_{\rm Sagn} = |f_- - f_+|$, we have the formula [1–3]

$$\delta f_{\rm Sagn} = \frac{4\mathbf{A}\mathbf{\Omega}}{P\lambda}\,, \tag{1.1}$$

where $\mathbf{A}\mathbf{\Omega}$ is the scalar product of the ring surface vector and the angular velocity of rotation, λ is the wavelength of optical radiation at frequency ν, and P is the circumference of the ring.

An estimate of the minimum detectable rotation speed (for a ring fed by an external optical pump) can be obtained by comparing the mode shift with the linewidth of a quantum generator (laser) (the so-called Schawlow–Townes formula)

$$\Delta f_{\rm q} = \langle \Delta f^2 \rangle^{1/2} = \frac{\nu}{Q}\left(\frac{h\nu}{\eta W t_{\rm m}}\right)^{1/2}, \tag{1.2}$$

where Q is the optical quality factor of the cavity, h is Planck's constant, η is the quantum efficiency, W is the pump power, and $t_{\rm m}$ is the measurement time.

The mode shift ('Sagnac splitting') detection condition $\delta f_{\rm Sagn} \geqslant \Delta f_{\rm q}$ yields formulas for calculating the detected rotation speed or for estimating the required ring radius for a given Ω:

$$\Omega \geqslant \frac{c}{2RQ}\left(\frac{h\nu}{\eta W t_{\rm m}}\right)^{1/2}, \tag{1.3a}$$

$$R \geqslant \frac{c}{2\Omega Q}\left(\frac{h\nu}{\eta W t_{\rm m}}\right)^{1/2}. \tag{1.3b}$$

A typical choice of parameters for an ideal external optical pump laser is as follows: $W \approx 1$ mW, $\eta \sim 1$, $\nu \approx 3 \times 10^{14}$ Hz, and $Q \approx 10^{10}$ (with a 10^3 finesse). To detect a slow rotation of the order of Earth's angular velocity $\Omega_{\rm E} = 7.3 \times 10^{-5}$ rad s^{-1}, we then obtain the ring size estimate

$$R \geqslant 3 \times 10^{-2}\, t_{\rm m}^{-1/2}\ [{\rm m}]\,,$$

which shows that the problem is already solved by a small-radius ring.

But much larger ring sizes are required: to register extremely small variations in angular velocity $(10^{-8} - 10^{-10})\Omega$,

$$R \geqslant 3 \times (10^2 - 10^4) t_{\rm m}^{-1/2}\ [{\rm m}]\,,$$

which shows that, even with a measurement time of the order of a day ($t_{\rm m} = 10^5$ s), ring cavities would be required that exceed the laboratory scale $R > (1-100)$ m. We note that relative variations in the angular velocity $\Delta\Omega/\Omega \sim 10^{-9}$ correspond to the possibility of measuring the fundamental harmonics of terrestrial tidal deformations with an accuracy of the order of 1%.

The need for large 'Sagnac rings' in order to detect weak gravity-inertial effects in terrestrial conditions was already clear to the pioneers of these studies, including Michelson (see details in [3, 4]). However, subsequent experiments with prototypes of large rings showed that there is an optimum size at which a compromise is achieved between increasing the sensitivity of the device and increasing noise interference due to the loss of rigidity of large structures [5].

In the foregoing, the Sagnac ring is represented as an inertial device: an accelerometer of rotational accelerations. But formula (1.1) shows that on Earth's surface it can also be a sensitive deformation sensor that registers the inclinations of its platform, because $\delta f_{\rm Sagn}$ depends on the angle between the axis of rotation and the normal to the surface of the ring. The classical pendulum 'tiltmeter' measures the angle between the normal and the plumb line — the vector sum of the gravitational force and the rotational inertia force (three orders of magnitude smaller). The simultaneous use of both instruments in principle allows separating these forces and obtaining more detailed information about geophysical perturbations [3, 5, 6].

We thus see that the geophysical applications of a large-size Sagnac gyroscope can be much broader than the actual problem of monitoring variations in Earth's rotation axis. Generally speaking, this includes measurements of the internal geodynamics of masses that make up Earth, such as perturbations of tectonic plates on faults and oscillations of the inner solid core.

We make a special note of possible applications to problems of fundamental gravity: the need to measure the fundamentally relativistic Lense–Thirring effect in Earth's field [7]. This is a specific precession of Earth's axis associated with the difference between the gravitational field of a rotating spherical mass and that of a static (spinless) mass. The effect is of fundamental (heuristic) importance, extending the notion of 'relativity' (the absence of a preferred reference frame) to the Universe as a whole (see [8] for Mach's principle).

A more sophisticated installation — a large-size ring laser — can be used for the fundamental problem of searching for dark matter. In particular, by creating a strong magnetic field in a chosen sector of an annular light path, one can attempt to search for axions — hypothetical elementary particles that, according to modern quantum electrodynamics (QED), might be produced in the interior of the Sun and irradiate Earth (see details in [9, 10]).

The role that Sagnac rings can apparently play in combination with the classical Michelson interferometer is nontrivial. Today, there is a shared knowledge that such mixed designs are promising for creating a new (third) generation of gravitational wave detectors, not only because they can help suppress external seismo-Newtonian ambient noise but also (and perhaps especially) because they provide a realistic way to bypass the quantum limitations of the sensitivity of gravitational antennas.

As regards the sensitivity of the Sagnac rings themselves, it can be substantially improved by switching from optical interference of electromagnetic waves to an atomic interferometer based on 'matter waves' or on de Broglie waves. At present, this line of research has an obvious innovative character and is already supported by existing laboratory facilities.

Finally, the large and medium Sagnac gyroscope can be used as a unique tool (or a framework) for the development and refinement of a new technique for precision angular measurements known as the 'Sagnac goniometer' idea [3].

In this review, these applications are described in as much detail as possible. A description is given of the underlying logic and physics of such research (including some historical background) with substantiation of the scientific and practical significance of each direction. We give numerical estimates that show the feasibility of the tasks set. The current state and planned development of work are presented, and the prospects of obtaining the expected results are assessed. [1]

In what follows, we discuss (not necessarily in the same order)

— a brief theory of the Sagnac effect;

— measurements of temporal and spatial variations of Earth's rotation axis;

— measurements of geodynamical processes and seismic waves in Earth's crust;

— the detection of rotational effects of relativistic gravity;

— experiments to search for dark matter particles;

— an analysis of mixed Sagnac–Michelson interferometers as tools for quantum nondemolition measurements;

— the development of Sagnac gyroscopes based on cold atoms;

— new aspects of a precision technique of angular measurements.

The review is provided with an extensive (although not exhaustive) bibliography, whence the interested reader can draw upon the omitted details.

2. On the theory of the Sagnac effect

The Sagnac effect is currently understood and being studied fairly well. The scientific literature consists of several hundred publications, including the work of Einstein as one of the creators of the special relativity (SR) theory. We refer the reader to fundamental theoretical studies represented by reviews in *Physics–Uspekhi* by Logunov and Chugreev [11] and Malykin [12] (the latter contains an extensive list of references). In this section, we briefly address only those theoretical aspects of the Sagnac effect that are essential for understanding the applications discussed below.

The correct interpretation of the kinematic nature of the effect is currently considered to be as follows. In a stationary (laboratory) reference frame, the velocity $\mathbf{v}$ of a harmonic (monochromatic) electromagnetic (EM) wave propagating along a ring waveguide is a combination of its phase velocity $\mathbf{v}_{\rm ph}$ and the linear velocity of points on the circumference of the ring, which rotates about the symmetry axis with an angular frequency Ω. According to the SR addition law for velocities, we have

$$v_{\pm} = \frac{v_{\rm ph} \pm R\Omega}{1 \pm v_{\rm ph} R\Omega/c^2}\,, \tag{2.1}$$

where the $\pm$ signs correspond to waves propagating along and against the direction of rotation of a radius-R ring. Having different propagation speeds, the counter-propagating waves take different times to pass the circumference of the ring $P = 2\pi R$.

Using (2.1), we can easily calculate these times $t_{\pm} = P/v_{\pm}$,

$$t_{\pm} = 2\pi R\,\frac{1 \pm v_{\rm ph} R\Omega/c^2}{v_{\rm ph}\left[1 - (R\Omega/c)^2\right]}\,, \tag{2.2}$$

and then their difference

$$\delta t = t_{+} - t_{-} = \frac{4\pi R^2 \Omega}{c^2\left[1 - (R\Omega/c)^2\right]}\,. \tag{2.3}$$

At a low rotation speed $R\Omega \ll c$, we can neglect the second-order term in the denominator and obtain formulas used in practice in measuring the Sagnac effect. For the magnitude of the time shift and the corresponding phase difference, which determines the result of the interference of counter-propagating waves at a certain point of a splitter (which was used to produce them from an external radiation source) on a screen or photodetector, we obtain

$$\delta t = \frac{4\mathbf{\Omega A}}{c^2}\,, \quad \delta\Phi = \frac{8\pi\mathbf{\Omega A}}{c\lambda}\,. \tag{2.4}$$

Here, λ is the length of the wave propagating in a ring waveguide and A is the area of the ring. Formulas (2.4) are written in vector form in the general case where the normal to the surface of the ring $\mathbf{n} = \mathbf{A}/|\mathbf{A}|$ does not coincide with its axis of rotation (hence the scalar product $\mathbf{\Omega A}$).

[1] In this review, when describing the applications of ring laser interferometers, diverse terminology is used, mainly for literary purposes: the Sagnac gyroscope (SG), gyrolaser, Sagnac ring, ring laser, Sagnac gyrocompass, etc. In fact, all terms are equivalent, denoting the same physical object with different accents, understandable from the context.

This description of the Sagnac effect is academic in nature, referring to the abstract concepts of phase, the phase velocity of harmonic waves, and their interference. For a better (practical) understanding of the essence of the effect, it is useful to consider the case of two EM pulses counter-propagating in a ring interferometer; they travel with group velocities, which also must be calculated by adding the group velocity and the linear rotation velocity $R\Omega$ in accordance with the relativistic law. Sufficiently short pulses then arrive at the splitting mirror of the interferometer at different times without forming an interference pattern. The magnitude of the Sagnac effect is then characterized by the differences among the arrival times of the pulses, which is to be measured. The use of interference in the description involving harmonic waves is only a method for measuring the difference in arrival times, which is many orders of magnitude more accurate than other methods, thus increasing the sensitivity to the angular velocity of rotation. We recall that, in the absence of an optical medium, the phase and group velocities of light coincide (i.e., the pulses do not spread, allowing the interpretation of point-like objects or test bodies).

Further, we see from formula (2.3) that the differences among the times spent by the counter-propagating waves for the passage of the ring is independent of the phase velocity of the waves. This means that the time difference due to the Sagnac effect is independent of whether the ring interferometer is filled with an optical medium. We hence conclude that, for waves of an arbitrary type (e.g., acoustic), the differences among the arrival times is the same (with the same wave parameters). Consequently, the Sagnac effect is universal in relation to the nature of objects propagating along the ring, be it harmonic waves, solitons, or particles. This is a purely kinematic effect.

If a material body constitutes an atom or an elementary particle and it corresponds to a de Broglie wave, then 'matter waves' or an 'atomic interferometer' and quantum interference of wave functions can be used to register the Sagnac effect [13].

We return to the proof of the kinematic nature of the effect, which is based on the SR velocity addition formula (2.1). However, SR was formulated for inertial reference frames (moving uniformly and rectilinearly relative to each other), and a rotating platform on which an annular waveguide is located is not such a system. The analysis of phenomena in noninertial reference frames involves the use of GR in general [14, 15]. For purely kinematic effects, however, the use of GR is not necessary. Following [12], we quote Einstein [16]: "The kinematical equivalence of two coordinate systems is not actually limited to the case where the systems K and K′ move uniformly and rectilinearly. This equivalence from a kinematical point of view also holds well, e.g., if one system rotates uniformly relative to the other." In the absence of gravitational fields, when there is no spatial curvature, noninertial reference frames can be described using SR for arbitrary accelerations [16, 17]. In [11], such an approach to the calculation of the Sagnac effect was implemented in a reference frame corotating with a ring interferometer. For calculations, the Minkowski-space metric tensor with a vanishing curvature tensor was used.

We next discuss the issue of using GR in calculations. In the GR framework, the Sagnac effect was in fact (albeit not named so) calculated in the *Course of Theoretical Physics* by Landau and Lifshitz [18], where the metric tensor is used to calculate the difference between the propagation times of counter-propagating waves in the corotating reference frame in the absence of an actual gravitational field (space–time curvature). The metric components in the rotating system are calculated from the interval invariance condition (the same was done in [11]). The result is given by formulas for the time and phase shift of counter-propagating waves, similar to (2.4). The results of calculations in GR [18] and SR [11] therefore coincide, and the question of choice does not arise. But in the presence of actual gravitational fields, expressions for the metric components include additional terms corresponding to these fields, and the integral magnitude of the Sagnac effect can only be calculated using GR. The same is needed if the ring interferometer rotates not uniformly but with a significant angular acceleration [19, 20], such that the angular velocity changes significantly during the time the counter-propagating waves travel around the ring. Here, too, it makes more sense to use GR.

At the same time, a particular circumstance forces us to pay more attention to the use of GR in Sagnac gyroscope calculations. This is the special role of rotation effects in the theory of gravity associated with the gravitational field of a rotating mass — the Lense–Thirring (LT) effect [21] — and Mach's principle (MP) [8, 22]. According to MP, the property (field) of inertia of bodies is the result of the action of gravitational accelerations from the masses of the ambient Universe (in accordance with the principle of equivalence of inertia and gravity). This should apply to both linear accelerations and rotational accelerations. The GR solution for the gravitational field of a rotating mass gives an LT correction that distinguishes the field from that of a static mass. According to MP, a corresponding correction should also be present in the inertial field induced by the relative rotation of the Universe. Obviously, there is a difficulty in the calculation, because superluminal relative velocities appear in considering the relative motion of distant masses with respect to a rotating reference frame, and therefore the calculation of the LT effect from MP becomes impossible. Apparently for the same reason, Einstein subsequently abandoned MP. However, among the fundamental applications of ring gyrolasers based on the Sagnac effect, there is a project to detect the LT effect in the gravitational field of rotating Earth. Obviously, the analysis and design of such an experiment require calculations of the Sagnac effect within the mathematical apparatus of GR.

To conclude this section, we mention that, in the extensive literature devoted to the Sagnac effect, there are various explanations of its nature associated with the action of centrifugal and Coriolis accelerations, Doppler and Aharonov–Bohm effects, and so on. A detailed analysis of alternative derivations and a bibliography is contained in review [12]. Here, we adhere to the kinematic nature of this effect, which we believe is obvious in the SR framework.

3. Measurement of the angular velocity of Earth's rotation

Currently, the parameters of Earth's rotation are measured by space geodesy methods using very-long-baseline radio interferometry (VLBI), satellite laser ranging (SLR), the global positioning system (GPS), and Doppler orbitography and radiopositioning integrated by satellite (DORIS). Over the past decades, an accuracy of 0.01 ms has been achieved for a measurement time of the order of one day and 0.1 arc ms in polar coordinates [23]. The general principle is to measure the

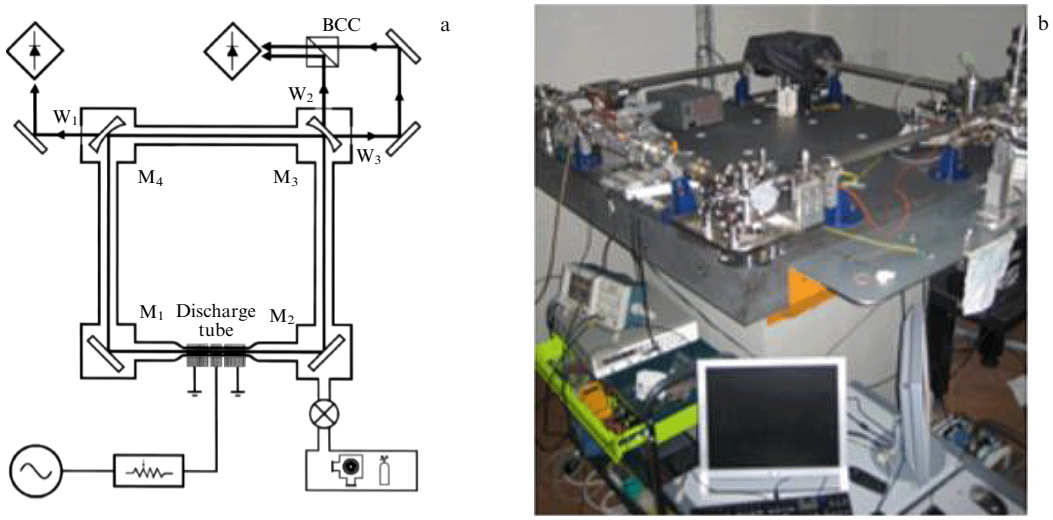

Figure 2. (Color online.) (a) Schematic of G-Pisa laser gyroscope with autopumping (square with perimeter of 5.60 m and area of 1.96 m^2): BCC — splitting cube, $W_1 - W_3$ — output beams, $M_1 - M_4$ — mirrors. (b) Photograph of G-Pisa setup.

rotation relative to the reference points of the most distant visible objects, quasars, using either the Global Navigation Satellite System (GNSS) or spacecraft (SC) outside Earth. All these methods are very complex and cumbersome: they require global networks and infrastructure for joint observation and data processing, coordinated by the international services IVS (International VLBI Service for Geodesy and Astrometry), ILRS (International Laser Ranging Service), IGS (International GNSS Service), and IDS (International DORIS Service).

An entirely different strategy is used to monitor rotation with inertial sensors. Previous mechanical gyroscopes, which actually measured the Coriolis acceleration, were not sensitive enough to detect small changes in Earth's rotation. Laser gyroscopes are based on the Sagnac effect, i.e., on the dependence of their modes on the angular velocity of rotation of the device. Optical interferometry, owing to the short wavelength of laser radiation, allows obtaining an extremely high resolution. Such a laser gyroscope, rigidly fixed on Earth, allows instantly controlling Earth's rotation and the spatial orientation of Earth's axis. To determine the total rotation vector, three independent linear laser gyroscopes are required in three mutually perpendicular planes.

Let us recall that the main tasks of monitoring Earth's rotation were (a) the detection of short-term spin oscillations with an accuracy of $10^{-9}\Omega$ and (b) the detection of short-term polar shifts with an error of 0.2 arc ms (or 6 mm). It is of interest to obtain such data in real time with a time resolution of 1 h or less. At the current stage, laser gyroscopes do not achieve the high long-term stability of VLBI radio astronomy networks. However, of independent interest are measurements at short time intervals, which are still difficult to access by cumbersome space methods. In addition, measurements made with ring lasers are continuous, while VLBI and SLR usually have measurement intervals of one day and gaps of several days or more.

There are plans to upgrade the VLBI network by replacing its radio telescopes with more modern ones (see https://ivscc.gsfc.nasa.gov/ar2008/V2C-PR_pagnum.pdf). The new worldwide network VGOS (VLBI Global Observing System) will be able to perform coordinate measurements with an order of magnitude greater accuracy and in less time. The prospects of new precision astrometry are available from the Internet resource http://sai.msu.ru/ao/documents/zharov.pdf.

Studies of the possible use of large laser gyroscopes in measuring geodynamical perturbations have been active for more than 50 years. Apparently, the first experimental work on the use of an He–Ne ring laser for detecting Earth's rotation is presented in [24]. Since then, considerable experience has been accumulated in constructing and operating about a dozen experimental installations of this type. Significant progress has been made in understanding the physical and technological features of their functioning. The goals and a realistic schedule for gradually achieving them have been formulated. In Section 3.1, we present the current state of development of this technology using the example of a medium-scale laser gyroscope, the G-Pisa ring gyroscope [25, 26], designed to control the geophysical vibrational background in the area where the Virgo gravitational interferometer is located. The historical background and a brief description of previous studies are given in Section 3.2. In Section 3.3, we describe the modern instrument itself, the G-Ring laser.

3.1 G-Pisa gyrolaser

G-Pisa is a meter-size installation (a square with a perimeter of 5.60 m, area 1.96 m^2) (Fig. 2). A lightguide made of stainless steel tubes has an adjustable modular structure with four mirror holders located at the corners, with a total volume of about 5×10^{-3} m^3. Like most geodetic (and navigation) optical ring gyroscopes, G-Pisa is an active optical device, i.e., radiation is generated inside the ring as in helium–neon lasers (in contrast to the passive version with external pumping). The vacuum chamber is completely filled with He together with an equal-isotope mixture of ^{20}Ne and ^{22}Ne. The total pressure of the gas mixture is 560 Pa with a partial Ne pressure of 20 Pa. Located in the center of one of the tubes is a discharge tube — an insert made of a Pyrex capillary with an inner diameter of 4 mm and a length of about 15 cm. The average radiation power in the lightguide is $W \sim 10^{-7}$ W; the wavelength is $\lambda =$ 632.8 nm.

For an active ring laser gyroscope, the formula for the limit sensitivity to angular velocity can be written as [25, 26]

$$\Omega \geqslant \frac{c}{2\pi KL}\left(h\nu\mu\,\frac{T}{2Wt}\right)^{1/2}, \tag{3.1}$$

where L is the side of a square-shaped contour, μ is the total loss in the cavity, T is the transmission factor of each mirror, W is the total power of the radiation coming out of the cavity, t is the observation time, and K is the scale factor of the device, depending on its geometry and wavelength (for a square-shaped cavity and $\lambda = 632.8$ nm, we have $K = 1.58 \times 10^6$).

A comparison with formula (1.3a) for a passive ring shows a correspondence between the factors $(2\pi KL)^{-1}(\mu T)^{1/2}$ and $(2RQ)^{-1}$, which, with the parameter values $L \sim R \sim 1$ m, $\mu =$ 40 ppm (parts per million), $T = 0.2$ ppm, $W = 5 \times 10^{-8}$ W, and $Q = 10^{12}$ (sharpness 10^5) adopted in calculations, have the same order of magnitude, $\sim 10^{12}$.

Substituting these values into formula (3.1) estimates the sensitivity of the G-Pisa instrument at a level of 10^{-9} rad s^{-1} Hz$^{-1/2}$; however, reaching the level of 10^{-11} rad s^{-1} Hz$^{-1/2}$ requires a device larger than 2 m in size.

In practice, the measured low-frequency output power spectrum (below 1 Hz) was typically of the order of 10^{-8} rad s^{-1} Hz$^{-1/2}$, which shows the sensitivity level actually achieved. During very quiet periods of the day, individual G-Pisa measurements showed improved sensitivity ($\sim 3 \times 10^{-9}$ rad s^{-1} Hz$^{-1/2}$).

For stable operation without disruption of the chosen settings, active perimeter control circuits were used in G-Pisa, which locked the δf_{Sagn} frequency to a reference laser. For this, two output beams of waves propagating clockwise and counterclockwise (taken off from one of the mirrors) were subjected to interference on a 50% beam splitter and were registered by a photodiode. After filtering and amplification, the output of the photodiode served as the control voltage for perimeter adjustment.

We note that the two counter-circulating output beams could also be used as independent modes. After their synchronous detection on the mixer, the beat frequency is extracted, which is actually a measurement estimate of Earth's rotation frequency. However, the main interest is in measuring its variations with the highest possible accuracy.

3.2 Large-area geodetic gyrolasers

A pioneering installation with a large laser gyroscope for astrogeodynamical measurements was assembled at the University of Canterbury in Christchurch (New Zealand) [3]. The Canterbury Ring (C-I) covered an area of approximately 0.75 m^2 and had a splitting frequency of nearly 71 Hz. It was the first underground ring laser to demonstrate counter-propagating mode splitting due to Earth's rotation (http://www.phys.canterbury.ac.nz/research/laser/ring_c1.shtml). The mechanical design of the device turned out to be insufficiently rigid, not permitting continuous monitoring over long time intervals. Then, with the participation of American and German scientific groups, another variant with improved long-term stability, C-II, was created (the main blocks were manufactured by Carl Zeiss in Oberkochen, Germany). The key technologies consisted of the use of a glass–ceramic zerodur as a support material for the lightguide for geometric stability and optical contact in mirror mounts in order to obtain a perfect vacuum seal. A photo of C-II is shown in Fig. 3. Since 1997, C-II has been operating 30 meters underground in a former World War II bunker called Cashmere Cave, located in Cashmere, a suburb of Christchurch. This instrument has a Sagnac splitting frequency of 79.4 Hz and is already capable of long-term observations. On segments having a constant atmospheric pressure, the Allan dispersion of the Sagnac frequency decreases from 1×10^{-5} to 5×10^{-7} with an averaging time of 700 s (details of the C-II design are considered in [3, 27]). But it turned out that the size of 1 m^2 is still small for detecting weak perturbations in Earth's rotation. In addition, an unpleasant problem of 'small rings' was the discovered connection between counter-propagating optical waves due to the backscattering of laser radiation from cavity walls. Backscattering is undesirable, because it makes the instrument extremely sensitive to random changes in circumference, for example, caused by variations in air pressure. This effect significantly decreases as the size increases. After that, the technology of geodetic laser gyroscopes was developed for a number of years at the same location, the University of Canterbury, but with the ideological and technological support of the University of Oklahoma, FESG (Fire Engineered Solutions Ghent) (USA), the University of Munich, and the Federal Office for Cartography and Geodesy (Bundesamt für Kartographie und Geodäsie (BKG)) (Germany).

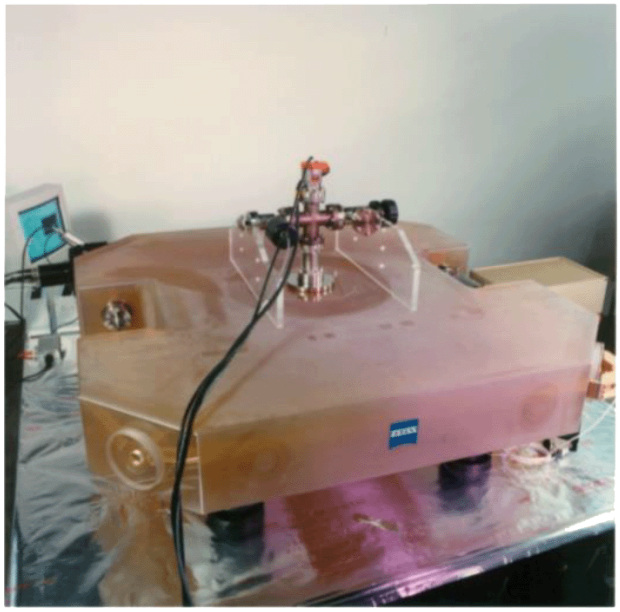

Figure 3. (Color online.) C-II Installation. Zerodur monolith, He–Ne laser (632.8 nm).

An important question investigated first was whether a large ring laser that would operate in the single-mode regime can physically be realized. A priori, this was not clear because, as the size increases, the free spectral range decreases and 'monoillumination' of only one mode becomes difficult; in addition, the optical power per individual mode decreases. To test the validity of this argument, a large but construction-wise simple 3.5×3.5 m ring laser was built on a vertical concrete wall in the Cashmere Cave [28] (Fig. 4). This prototype, called G-0, which became operational in 1998 with a radiation power of about 10 μW, had an expected Sagnac frequency of 288 Hz. The G-0 parameters were monitored over many years of observations in order to

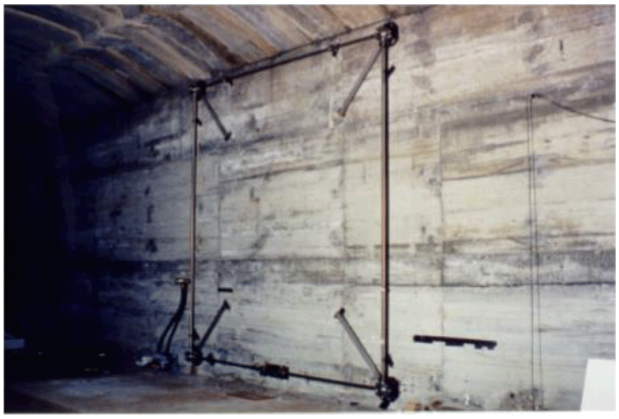

Figure 4. Installing G-0 on a concrete wall in the Cashmere Cave.

study the stability of this type of instrument. At the same time, a 'gigantic' He–Ne laser UG1a with a rectangular cavity 21×17.5 m in size was designed and built in the same cave [29] (the suffix 'a' in the UG1a name indicates the absence of vacuum pumping of the light guide).

The UG1a installation was designed in order to perform a relatively inexpensive test of whether any fundamental obstructions block the path to the ultimate goal of building an active ring laser large enough to measure the angular velocity of Earth's rotation at a 10^{-9} level with an integration time of 1000 s. The installation was upgraded to the UG2 version with an evacuated light path and an increased size, 21×40 m [30], which still fit in the Cashmere Cave bunker (Fig. 5). The contour area was about 835 m^2 and the Sagnac frequency was 2180 Hz. In all installation versions (G-0, UG1, and UG2), the radiation power circulating in the circuit was low, about 10^{-8} W. At such a power, there is no mode locking that destroys the Sagnac splitting due to weak coupling of modes. Synchronization could also occur due to external interference resulting from contact with the cave floor in the absence of negative feedback loops. The operation of these instruments at a very high sensitivity level (~ 10 prad s^{-1} $Hz^{-1/2}$) testifies to the stability of conditions in the Cashmere Cave itself.

In hindsight, installations involving 'giant Sagnac contours' in Christchurch encourage mentioning the experience of the pioneering pathfinders, the creators of SR themselves. Back in 1925, in a suburb of Clearing (Illinois, USA), A Michelson and N Gale measured the speed of Earth's rotation with a giant optical interferometer configured as a rectangular Sagnac contour (334×603 m^2) [4]. The experiment consisted in comparing the observed output grid pattern with the one calculated from the geometry of the interferometer (the title of paper [4] was "The Effect of the Earth's Rotation on the Velocity of Light"). Of course, in connection with the problem of the absolute reference frame (ether), the authors were interested in the difference between the speeds of light waves in the direction along and against the diurnal rotation of the interferometer. But their formula coincided with the Sagnac formula, and the result obtained confirmed the astronomical measurements of Ω to within 2%.

Returning to the gigantic installations in Christchurch, we note that they were created following the maxim "the more the better." However, these lasers have not realized their potential due to an unexpected increase in losses on the mirrors inside the cavity and the vulnerability to geometric

Figure 5. (Color online.) Photograph of UG2 prototype in the Cashmere Cave bunker.

changes (instability) of the design as a whole [31]. As a result, an important lesson was learned regarding the optimum size of a ring laser gyroscope rigidly attached to Earth (at least until active scale factor stabilization is involved). This size approached 3–5 m, which was in good agreement with the G-Ring Laser project for the creation of a 4×4-m ring laser gyroscope [28]. The contract between the Max Planck Institute of Quantum Optics (MPI) and BKG with Carl Zeiss for the construction of a large ring laser G was signed in September 1998. The facility was officially commissioned in October 2001.

3.3 G-Ring Laser installation

The G-Ring Laser (GRL), the best among the operational installations, is located at the Geodetic Observatory Wettzell (Bavaria) (www.fs.wettzell.de) (Fig. 6). Structurally, the large ring laser G is similar to C-II. It is also made of zerodur glass ceramic, but in a semimonolithic design. Four rectangular rods (strips) made of zerodur glass and rigidly attached to a round granite slab hold a square light conductor with a square side length of 4 m (Fig. 7). The thermal expansion coefficient is 1.4×10^{-8} K^{-1} for the base plate and 1.7×10^{-8} K^{-1} for the rods, resulting in the overall coefficient of $\sim 1 \times 10^{-8}$ K^{-1}. Four mirrors and their holders are attached to the front sides of the rods by molecular adhesion (optical contact). This technique provides a reliable vacuum seal. After the installation, the mirrors cannot be adjusted. The only way to adjust the modes is to control the tilt of the incoming beam and the pump intensity. The mirrors are of extremely high quality; low losses (several ppm) reduce backscattering to a non-critical level. The mirrors are slightly concave with a curvature radius of 4 m to axially hold the beam. The active medium, a helium/neon gas mixture with a pressure of about

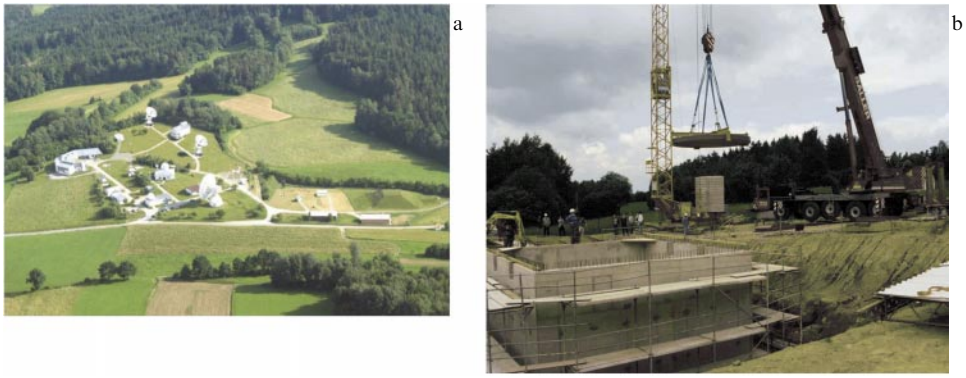

Figure 6. (a) Wettzell Geodetic Observatory (MPI, Germany). (b) Pit at the GRL installation.

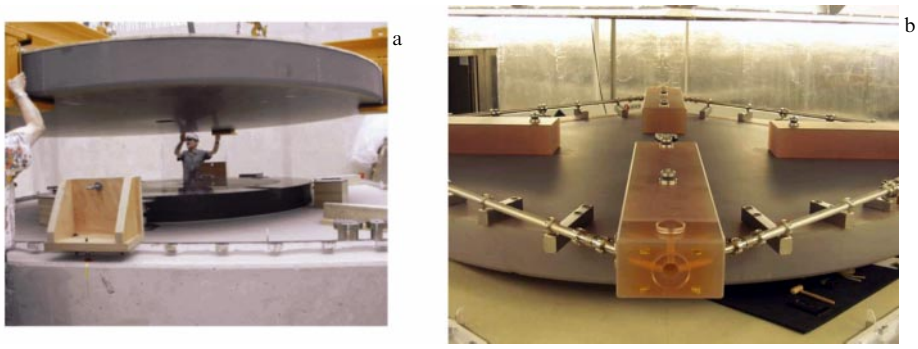

Figure 7. (Color online.) (a) Mounting a granite base plate at the GRL installation. (b) Mounting zerodur rods onto the GRL base plate.

10 mbar, is excited by a discharge in a pyrex gain tube by an alternating electric field with the subsequent monitoring of the generation process. The power of the optical beam is kept constant by a feedback loop that controls the excitation process. The key parameters of the GRL setup are as follows: Sagnac splitting frequency of 348.6 Hz and optical power circulating in the circuit $\approx 10^{-8}$ W.

3.3.1 Environmental noises. The G-Ring laser, as mentioned above, is mounted on a polished granite slab embedded into a concrete pedestal weighing 90 tons. The pedestal is attached to a massive concrete pillar 2.7 m in diameter, placed on a stone base lying 10 m below (Fig. 8). A system of concrete rings and insulating materials protects the pedestal and the pillar from lateral deformations and heat flows. The installation is already protected from external influences by its underground location. Its passive thermal stability is achieved with a two-meter alternating layer of expanded polystyrene, wet clay, and four meters of bulk soil. A side entrance tunnel with five insulating doors and a separate control room minimizes thermal perturbations. After two years of thermal adaptation, the average temperature reached 12.2 °C with seasonal fluctuations not exceeding 0.6 °C. However, despite the serious measures taken to ensure the stability of the foundation, the GRL installation failed to completely eliminate tilts due to soil deformations of thermoelastic or hydrological origin at the level of ~ 1 μrad. This hindrance seems to be impossible to eliminate in principle. Tilts in the north–south direction mask the measured rotation signal of Earth and must be compensated for. For this, tilt sensors are installed at the outer ends of the zerodur rods that hold the GRL light guide; two more sensors are placed near the center of the base granite slab (in total, there is a set of six Lippmann-type tilt sensors). The high resolution of these devices and the conservative environmental conditions allow detecting tilts at the level of ~ 1 nrad and taking them into account in data processing. Other environmental parameters, such as the temperature at different points of the shelter, air pressure and humidity, and the groundwater level in the installation area, are detected and recorded once a minute.

3.3.2 Frequency stability. For the Sagnac frequency, according to formula (1.1), the scale factor (the coefficient of conversion of rotation into mode splitting) increases with ring laser size. But the resolution of the device (the minimum detected splitting) is fundamentally limited by the quantum photon noise of laser radiation. Its level can be estimated using information about the quality factor of the cavity, measured from its 'ringing' time, and optical power (1.2). This leads to an estimate of the maximum sensitivity of the GRL setup of $\sim 9 \times 10^{-11}$ rad s^{-1} Hz$^{-1/2}$. To achieve the resolution $\Delta\Omega/\Omega \sim 10^{-9}$ in terms of Earth's rotation speed (or 7.3×10^{-14} rad s^{-1}), an integration time of 420 h (15 to 20 days) is needed. At the Geodetic Observatory Wettzell facility, this is difficult to achieve due to instrumentation drifts.

A practical parameter for evaluating the resolution and stability of a ring laser is the Allan variance σ_A^2 of the Sagnac splitting frequency. This quantity describes the dispersion of frequency variations in a time interval of a given length (the averaging time). It also helps identify the nature of noise processes: white noise, $1/f$ flicker noise, etc. The GRL resolution at short times (up to 5000 s) is limited by white

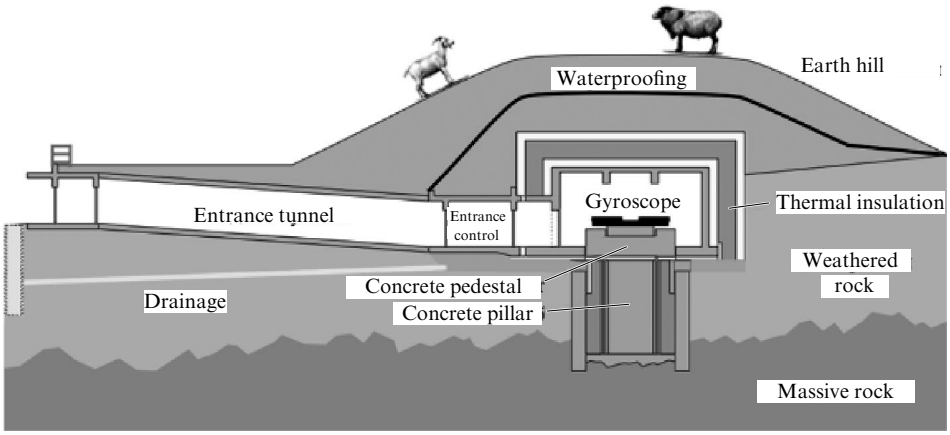

Figure 8. Layout of GRL with environmental protection.

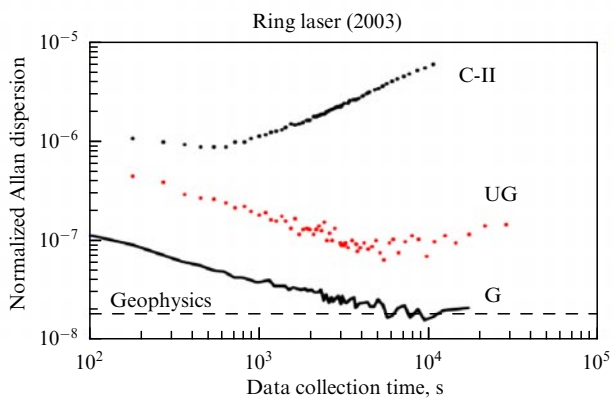

Figure 9. (Color online.) Allan variance for three types of ring SGs.

noise and, probably, shot noise, showing a characteristic slope $t^{-0.5}$ on the logarithmic plot of the Allan variance. The Allan deviation reaches a minimum at an averaging time close to 2 h and then increases again, which is a consequence of the nonstationarity of the noise (so-called instrumentation drifts). After removing periodic components from the record, such as the effect of terrestrial tides and the daily movement of the pole, the relative minimum of the Allan deviation (the level of experimentally observed noise) is reduced to $\sim 10^{-8}$ for averaging intervals of the order of 3 h. At such time intervals, the resolution of the GRL setup in terms of Earth's rotation variations is $\Delta\Omega/\Omega \sim 10^{-8}$.

To conclude this section, we present comparative Allan variances for three types of geodetic ring (large-size) interferometers, which were presented above as instruments for measuring Earth's rotation (Fig. 9).

3.3.3 Observation of Ω oscillations. The installation in Wettzell has been operating for almost 20 years since its official launch and about 10 years after an upgrade to the design sensitivity. It is interesting to look at the results of observations of the angular velocity of Earth's rotation. We first recall the effects observed at the facility: short-period tidal harmonics (primarily due to the influence of the Moon and the Sun), harmonics with a period of the order of a year generated by perturbations of Earth's orbit, atmospheric and oceanic processes, and, finally, long-period 'secular' oscillations of Earth's axis like free Chandler oscillations [32].

The spectrum of tidal components contains oscillations with periods of 13.7, 27.3, 9.1, and 7 days [33]; it is therefore possible to observe beats in GRL signals with periods of 10 days or less. By order of magnitude, these effects can be estimated by multiplying Earth's rotation speed of $\sim 7 \times 10^{-5}$ rad s^{-1} by the relative fraction of the tidal potential of $\sim 10^{-7}$. The estimate gives the amplitudes of rotation variations at the level of several prad s^{-1}. Their detection is already possible with the 'Allan stability' equal to 10^{-7}. The period of Chandler oscillations is ~ 14 months (435 days), and the order of the induced deviations in the rotation speed can also be significantly higher, $\sim (20-40)$ prad s^{-1}. With these preliminary expectations in mind, we turn to the results of measurements at the GRL facility published in [34].

Figure 10 shows the experimental data of a large ring laser over a measurement period of 60 days. The total angular velocity variations are displayed with the constant component subtracted, corrected for local tilts of the ring (Fig. 10a), the calculated variations in the beats of tidal harmonics (Fig. 10b), and the 'Chandler walk' effect obtained from the data in Fig. 10a minus the data in Fig. 10b, on the background of Earth's rotation frequency drift (blue track) according to VLBI measurements. As the authors of [34] point out, in the course of these measurements, GRL operated with an active cavity length stabilization system. The noise level in Sagnac frequency measurements was about 2 prad s^{-1}, while the random drift was within 5 prad s^{-1}. The optical frequency of the laser was stabilized to within 60 kHz for three months.

In general, the quality of the installation over the specified period, in addition to the presence of some aperiodic variations in the residual signal, is characterized by a weak linear drift of 0.164 prad s^{-1} day^{-1} for almost 60 days. This is the highest level of inertial sensor stability that the G ring has ever achieved.

This example shows that the sensitivity and stability of large ring laser gyroscopes currently allow direct measurements of the combined Chandler effect and Earth's free-rotating annual frequency variation. The ring laser results are in good agreement with independent measurements of the VLBI system.

To conclude this section, we make the following remark. From the position of an external observer, the picture of space–time variations in Earth's axis is usually presented for clarity as shown in Fig. 11, which displays the precession cone, spatial oscillations of nutations, and the Chandler

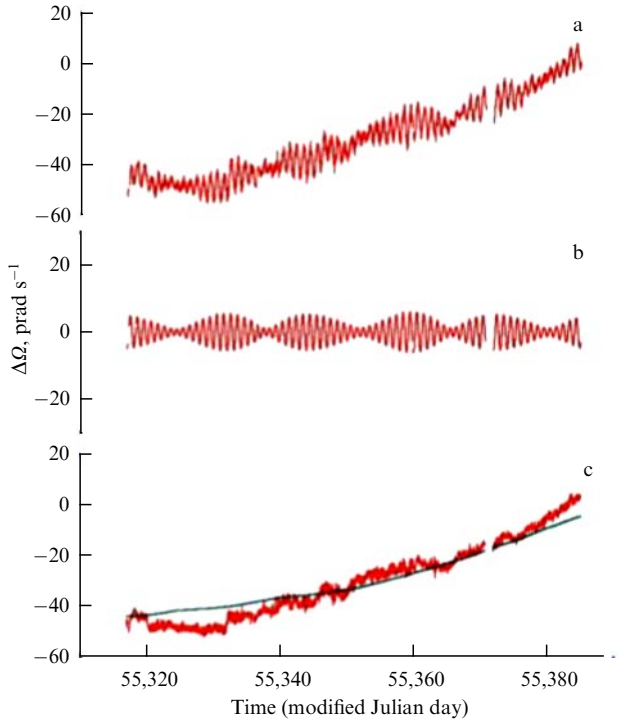

Figure 10. (Color online.) Records of variations in Earth's rotation at the GRL facility over 60 days in 2010. (a) Total angular velocity variations minus the constant component, corrected for local ring tilts. (b) Calculated variations in the beats of tidal harmonics. (c) Chandler walk effect deduced from results presented in panel a minus results shown in panel b, on the background of Earth's rotation frequency drift (blue track) according to VLBI measurements.

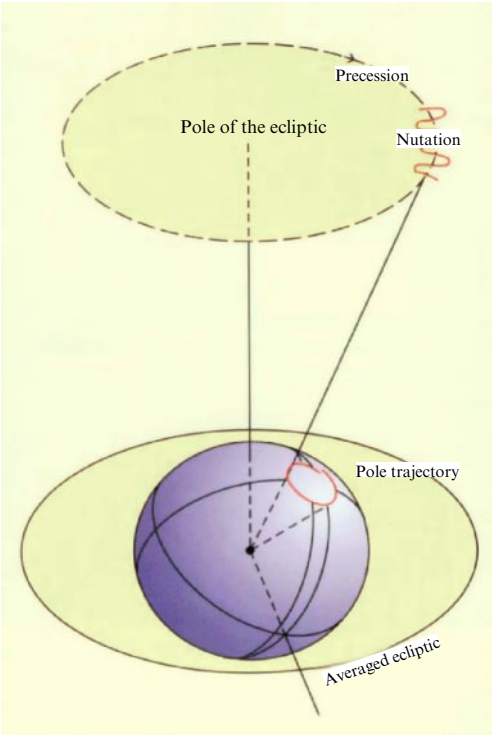

Figure 11. (Color online.) Generalized picture of variations in Earth's rotation axis. Shown: precession cone, spatial oscillations of nutations, and Chandler trajectory of the pole (red line on Earth's surface); period of 1.4 years.

trajectory of the pole (red line on the body of Earth), with a period of about 1.4 years. All of these are very slow processes (see [32, 33]): the precession period (time to go around its cone) is 25.7 thousand years (about 1° in 72 years), and the precession cone angle is 23°27′. The nutation ellipse period is 18.6 years and its angular size is 18.4″. Such variations could not be detected by the GRL setup in experiment [34]. Only tidal harmonic beats and the slow Chandler drift are present in the output signal pattern (see Fig. 10).

4. Measurements of seismic perturbations in Earth's crust

A gyrolaser is a tiltmeter, because it is sensitive to the inclinations of the ring plane with respect to the gravity vector. This means that seismic perturbations can also be registered by it. However, a gyrolaser is not a simple addition to the sensors already known in seismology. With its development, qualitatively new possibilities become available: the detection and measurement of toroidal modes of Earth's natural oscillations excited by earthquakes [35, 36].

4.1 Instrumentation complex for seismic monitoring

Two types of sensors are traditionally used in seismology. The first comprises standard inertial seismometers that measure the three spatial components of ground translation motion to monitor natural seismic activity and other perturbations. The second type, comprising differential instruments, is represented by strainmeters designed to measure relative displacements. There has long been a need for sensors of a third type, ground rotation meters for a complete description of motion at a given point on Earth's surface. The three components of seismically induced rotation were extremely difficult to measure due to the insufficient resolution of mechanical inertial seismometers, in particular, due to the large noise background over a wide range of frequencies and scales.

Modern geodetic ring laser gyroscopes provide control over the rotational motion of the soil. The first observations of Earth's rotational modes have already been made with a high frequency resolution, which is in demand for seismology. These achievements stimulate the emergence of a new field of geophysical research, which can be called *rotational seismology*.

4.1.1 Background on the object of detection. There are different types of seismic waves, but four are generally considered: compression or P-waves (primary waves); transverse or S-waves (secondary or shear waves); Rayleigh waves; and Love waves.

The first two types, P and S, are called body waves, because they propagate through the body of Earth. Waves of the last two types are called surface waves, because they propagate over the surface of Earth. Waves have different structural configurations and propagation speeds. In addition to the translation motion of the soil, they can also cause its rotational motion, with the exception of P-type waves, in which matter undergoes expansion and contraction. Shear waves and Rayleigh waves cause rotation in the vertical plane normal to the wave vector, while Love waves generate rotation in the horizontal plane. Conventional seismometers measure three components of linear displacement. However, a complete description of the motion of a medium requires information on all three components of rotation.

4.1.2 Seismic control devices. A modern seismic monitoring center is a classic seismic tracking station with a traditional set of displacement and deformation meters in a wide frequency range, but now with the addition of a geodetic ring laser gyroscope, which is a rotation meter. An example is the station of the Geodetic Observatory Wettzell, where, over several years, researchers managed to collect a comprehensive database of several hundred earthquakes with magnitudes ranging from M3 to M9 [5, 36].

A property of elastic wave fields known from seismology — phase synchronism of the transverse acceleration (seismometer) and of the induced rotation velocity (gyrolaser) [37] — allows obtaining information about the speed and direction of seismic waves from the results of measurements at individual localized points (objects) [36 , 37]. This property is used in the calculation of the inverse seismic problem, making it possible to implement seismic tomography of Earth in the absence of information about the travel times (delays) of remote signals [38, 39]. The developed technique can be used for a tomographic reconstruction of the structure of seismic velocities around receivers. The locality of this approach is effective for applications where there is no multicomponent network of sensors (for example, on the ocean floor, in remote areas, and in wells).

A significant upgrade (quality improvement) of the ring gyrolaser in Wettzell after 2009 led to the first experimental observation of free oscillations of Earth based on rotational perturbations from propagating seismic waves [40]. With the GRL, based on the records of several time series of giant earthquakes, it was possible to detect the propagation of Love waves around Earth in the form of a quadruple echo (repetitions of the signal of a wave traveling around Earth). This proves the effectiveness of this tool for detecting Love waves with a horizontal deformation structure. Attempts to record Love waves with seismometers give readings that are heavily contaminated by tilt motions [41].

Spectral analysis of recorded observations [36, 38] revealed the theoretically expected spectral lines corresponding to toroidal modes, which cannot be measured solely with seismometers and tiltmeters. It was ring lasers that began to fill this gap. The studies conducted raise the question of the efficiency of such observations for the analysis of the deep structure of Earth and the nature of seismic sources. In particular, a relation, observed in a number of past earthquakes, between the toroidal and spheroidal modes has been studied [42].

After upgrading and improving the signal-to-noise ratio of the large GRL gyrolaser, an oceanic signal appeared in its records on the background of environmental noise [43]. This success stimulates the development of a new approach — applying optical gyroscopes to the problem of the origin of the field of noise waves generated by the ocean. The ring laser, unlike seismometers, measures pure Love waves, but their origin and nature are not fully understood. The classical theory for the generation of oceanic perturbations predicts Rayleigh waves, but not Love waves [44]. To clarify this discrepancy, experimental studies of the Love wave sector in Earth's noise field must be continued with the use of gyrolasers.

4.2 Gyrolaser as an earthquake detector

Rotations caused by earthquakes have been neglected in standard seismology. The magnitudes of the corresponding signals were considered small, and no instruments with the required sensitivity were available. The high resolution of large ring lasers, along with their insensitivity to linear accelerations, changes the situation. Detection of remote seismic bursts (earthquakes) by rotational perturbations appears to be a promising technique. The expected range of measured variations in angular velocities is very wide, estimated as $10^{-14} \leqslant \Omega \leqslant 1$ rad s^{-1}, and the signal frequency range for surface seismic waves is $0.003 \leqslant f_s \leqslant 10$ Hz [45]. Ring lasers with different orientations can ensure detection of rotational perturbations from both Love and Rayleigh seismic waves. The sensitivity of the gyrolaser at the Wettzell station (2×10^{-11} rad s^{-1}) is sufficient for detecting waves of this type from distances of several ten thousand kilometers. In addition, this device is suitable for measuring weak perturbations in the seismic near field. For seismic applications of a ring laser, its long-term instrumental stability is not as important as in the problem of measuring Earth's rotation. More important for stable single-mode operation is the short-term accuracy and mechanical rigidity of the laser beam lightguide.

4.3 Detection of toroidal modes

Very strong earthquakes cause free vibrations of the planet that significantly exceed the background noise level. However, observation and correct interpretation of the spectrum of free oscillations by traditional seismic instruments are not easy tasks, especially for toroidal modes. Toroidal modes are difficult to observe, because, being superpositions of Love surface waves, they have a low quality factor compared with that of spheroidal oscillations and decay faster. As noted, Love waves, which have a horizontal structure, are difficult to filter at a high noise level in the records of horizontal seismometers. Finally, the horizontal components of the displacements are 'contaminated' with an admixture of oblique deformations of the surface, which leads to apparent translation motions exceeding the true ones [41]. Under these circumstances, the use of the readings of geodetic laser gyroscopes greatly simplifies the task of observing toroidal-type free oscillations of Earth.

To be specific, we recall the first time toroidal oscillations excited by a strong earthquake (Tohoku, Japan, 2011) were detected with the use of the GRL installation [40, 42]. On March 11, 2011, the devastating Tohoku–Oki earthquake with magnitude $M_W = 9.0$ occurred in the North Pacific Ocean, off the east coast of Honshu. With the help of the Wettzell ring gyrolaser, it was possible to detect trains of Love waves that circled Earth four times (in two opposite directions). Figure 12 shows seismograms of rotational motions of Earth's crust around the vertical axis, recorded using a ring laser (red tracks). In addition, seismograms of the transverse acceleration in the horizontal plane, recorded by a nearby STS-2 broadband seismometer (black tracks), are also shown.

Figure 12a shows time intervals of the records representing the first eight trains of Love waves, labeled G1–G4, and Fig. 12c shows time intervals of records of the next eight trains G5–G8. Signals G1, G3, G5, and G7 travel from the source to the receiver against Earth's rotation, 'along a short arc.' Signals G2, G4, G6, and G8 travel along the rotation direction, i.e., 'along a long arc.' Figure 12b shows the propagation paths of a Love wave along great-circle trajectories from the earthquake source to the receiver (for example, to the Wettzell gyrolaser). For G1, G3, G5, and G7, the shapes of the rotation speed and lateral acceleration

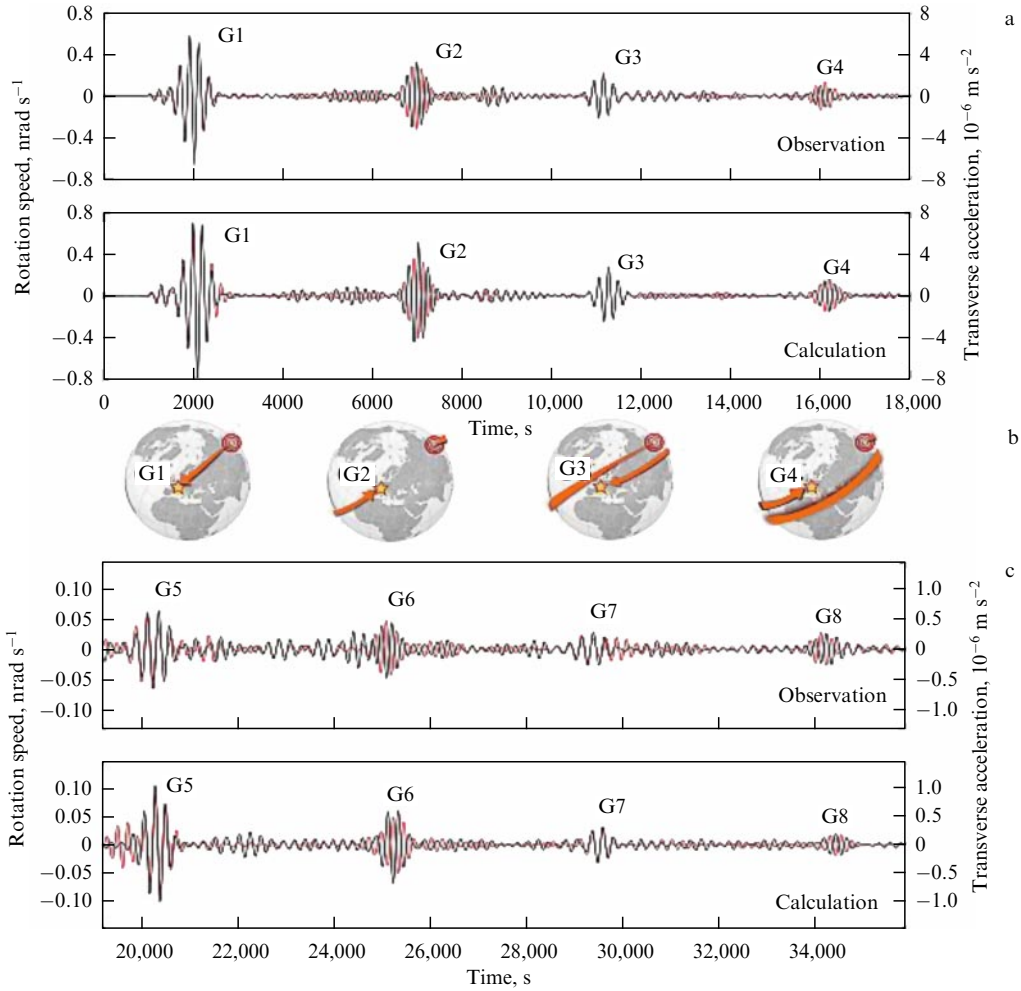

Figure 12. (Color online.) Registering the multicirculating passage of a Love wave by GRL (red track) and MET seismographs (STS-2) (black track) at the Wettzell Observatory (Tohoku earthquake, Japan).

signals are very similar. The G$(2n+1)$ $(n \geqslant 0)$ rotation speeds show a positive correlation with lateral accelerations. The ratio of the acceleration-to-rotation-speed amplitudes (according to the theory in [35, 46]) is approximately equal to twice the horizontal phase velocity, which is 4.5 km s^{-1}.

For sequences G2, G4, G6, and G8, the rotation speed and acceleration do not have the same phase, but have a reversed polarity. This is due to their reverse propagation direction.

Data spectra were also plotted for 48 h after the Tohoku event [42]. A comparison of the spectra of the observed modes is presented based on the records of the transverse acceleration of the WET (Wettzell) seismograph (Fig. 13a) and the records of Sagnac frequency variations (i.e., rotations around the vertical to the GRL ring plane) rescaled by a factor of 10,000 (Fig. 13b). The vertical lines indicate the frequencies of the principal spheroidal (red) and toroidal (blue) modes calculated for the PREM (Preliminary Reference Earth Model) with rotation. Similar patterns of multiorbital Love waves were also obtained in Wettzell for earthquakes in Maule (Chile) (2010) with $M_{\mathrm{W}} = 8.8$ and in the Samoa Islands (2009) with $M_{\mathrm{W}} = 8.1$.

This example shows that ring laser technologies have reached a level of sensitivity that offers an interesting addition to traditional seismological instruments, demonstrating advantages in observing long-period motions of Earth's surface and thus gaining insights into the dynamics of Earth's structure.

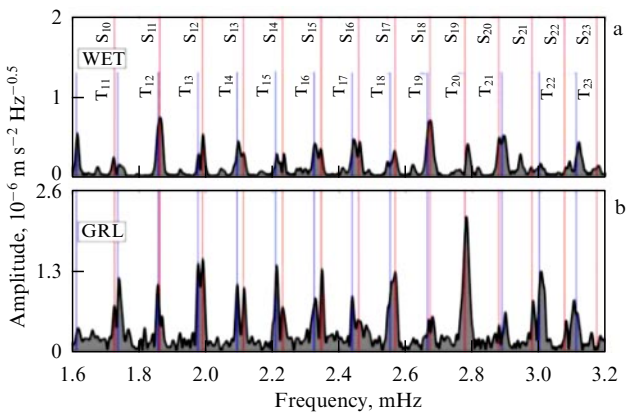

Figure 13. (Color online.) Spectra of Earth's oscillations recorded by (a) WET and (b) GRL seismographs after the Tohoku earthquake (Japan). S and T are spherical and toroidal modes.

Already in the short term, ring laser technology introduces a new type of ground motion control into seismology, with consequences that are not yet fully understood. The combination of these instruments with a

classic set of linear geophysical sensors endowed with an optical indication system (seismometers, gravimeters, and strainmeters) is a current trend in designing international scientific centers of the Global Geodetic Observing System (GGOS) [47].

5. Detection of GR rotation effects

The possibility of using large-scale gyrolasers for the experimental study of GR rotation effects (in particular, for measuring the differences between the gravitational field and the Newtonian one for spinning spherical masses) has been realized by now.

Measurements of this kind became a subject of attention a long time ago (in fact, immediately after the publication of theoretical studies by Lense and Thirring [21, 48]), as one of the most striking and characteristic effects of GR in comparison with the classic theory of gravity. Indeed, the difference between the fields of a resting and a rotating spherical mass is a fundamental effect, emphasizing a deeper insight into the nature of gravity in the relativistic approach. The conceptual significance of this phenomenon is also due to the role that rotation effects play in the problem of the existence of an absolute frame of reference, be it with or without recourse to Mach's principle [8, 49].

Before considering the prospects for ground-based gyrolasers designed for measuring relativistic effects of rotation, we briefly recall the successes of space missions devoted to this problem.

5.1 Orbital experiments

Space experiments have already been performed with the Earth satellites Gravity Probe-B [50] and LAGEOS 1 and 2 [51] (LAGEOS stands for LAser GEOdynamics Satellite), proving the existence of spin gravitational effects in the framework of numerical estimates following from GR.

The Gravity Probe-B (GP-B) mission, after 40 years of preparation, implemented the ideas of Schiff, the so-called Relativistic Gyroscope project, whose concept was proposed back in 1960 [49]. Implementation was undertaken by a team at Stanford University (W Fairbank and F Everitt) whose expertise was in the use of superconductivity in precision experiments; they were successful in initiating the mentioned NASA mission. The scheme of the space experiment was as follows. Four mechanical gyroscopes in the form of perfectly spherical quartz balls (with $\Delta r/r \sim 10^{-7}$) covered with a niobium film were placed in a cryostat on the satellite. The balls were placed in a superconducting suspension, each inside a spherical capsule (a walnut shell approximately 4 cm in diameter).

Superconducting currents in the niobium film created a magnetic moment collinear to the axis of rotation, whose orientation with respect to a fixed direction to a distant star was measured by quantum magnetometers (SQUIDs) using an onboard optical telescope. The reference star was chosen to be IM Pegasi (HR 8703), as a compromise between the degree of remoteness and sufficient brightness (stellar magnitude). The motion of the star itself was tracked by a ground-based VLBI network.

Two gyroscopes with axes lying in the orbit plane were used to detect geodesic precession. The other two, with the axes perpendicular to the orbit plane, served to detect the LT precession. The measurement scheme thus involved a mechanism for separating two types of precession.

The GP-B spacecraft was in the class of drag-free satellites with compensation for nongravitational perturbations. The spacecraft moved along a polar geodesic near-circular orbit with an altitude of ~ 640 km. Under these conditions, the magnitude of the effects predicted by GR was 6630 ms per year for the geodesic precession and two orders of magnitude less, 38 ms per year, for the LT precession.

The GP-B satellite was launched on April 20, 2004. The mission ended in September 2005, when the remains of the liquid helium evaporated in a cryostat (the initial volume was 2200 liters). Data processing and analysis were very time consuming and required constant attention from the team led by Everitt. Eventually, in October 2010, the GP-B team announced that the experiment had allowed successfully measuring both the geodesic precession and the LT precession (dragging of the gyroscope by a gravitational field of rotation). The result agrees with the GR prediction with an accuracy of 0.3% for geodesic precession and 20% for the LT effect [50] (i.e., 100 times rougher).

Another method for detecting the effect of frame dragging by a rotating gravitating body is to track the rotations of the orbital plane of near-Earth satellites. In fact, in this approach, a satellite is regarded as an equivalent gyroscope (spinning top) with the angular momentum normal to the orbit plane. The rotation of the central body introduces corrections into the satellite trajectory, which manifest themselves in a precession of its angular momentum vector around Earth's rotation axis. The idea of such an experiment, proposed by Van Patten and Everitt [54], was to measure the mutual deviation (drift) of the planes of the polar orbits of two counter-rotating satellites. According to the estimates in [54], the relativistic precession of these orbital gyroscopes must result in a relative displacement of the nodal points of the orbits at a level of 0.1 to 0.01 arc seconds per year. An attempt to realize the idea of the authors of [54] was made using the LAGEOS satellites, whose purpose was to study geodynamics and refine the parameters of Earth's gravitational field.

LAGEOS 1 was launched by NASA in 1976 [52], and LAGEOS 2, built by the Italian Space Agency, in 1992 [53]. Unlike GP-B, these are the simplest passive satellites, which reflect a laser beam sent from Earth. Thanks to laser ranging, the position of the satellites could be determined with high accuracy. Each satellite is a (nonmagnetic) brass ball 60 cm in diameter and approximately 400 kg in weight. For LAGEOS, the ratio of its mass to the cross-sectional area is much larger than for conventional spacecraft, and drag by the atmosphere has a much smaller effect on the orbit. Unlike GP-B, these satellites do not have any electronics, motors, power supplies, and so on. The presence of ferromagnetic elements was minimized to prevent the influence of Earth's magnetic field on the motion of the satellites. The brass ball was covered with a thin aluminum shell containing about 425 evenly spaced corner reflectors. The main goal was the precise tracking of the evolution of the orbit by laser ranging.

The orbits of both LAGEOS satellites were almost circular, with an eccentricity of 0.0135, perigee of 5620 km, and orbital period of 223 min. The task was to measure the relative precession, which, according to calculations, had an angular velocity of ~ 31 ms per year for the nodal points of the orbits. Ideally, according to the theory of the experiment in [54], the orbits of both counter-rotating satellites should have mutually complementary inclinations, compensating the dominant (126 degrees per year!) nodal precession caused by Earth's Newtonian multipole moments. Unfortunately, the

LAGEOS 1 and 2 satellites were not launched in precisely compensating orbits, which greatly complicated data processing and filtering the LT effect. Nevertheless, the Ciufolini group [55, 56] that performed the analysis combined the LAGEOS 1 and 2 nodal precession data with improved models of Earth's multipole moments (obtained by two orbiting geodetic satellites: CHAMP (CHAllenging Minisatellite Payload) and GRACE (Gravity Recovery And Climate Experiment)), and reported a 10% confirmation of GR [57]. Later, the Italian Space Agency launched a third satellite, LARES (LAser RElativity Satellite), also with laser-ranging control [58]. The inclination of LARES is very close to the required complementary angle for LAGEOS 1. Combining the data from all three satellites, it will apparently be possible to measure the LT precession with an error of 1% [58]. Additional comments on the GP-B and LAGEOS 1 and 2 experiments can be found in critical review [59].

As regards astrophysical tests of other types, we recall the long-known idea that the LT precession can be detected from the dynamics of a system of relativistic binaries involving black holes or neutron stars whenever a pulsar component is present in the system [60].

5.2 Ground-based measurements with large Sagnac gyroscopes

We return to the possibility of detecting relativistic effects of rotation in terrestrial conditions using large laser gyroscopes. The advantage of this method lies in the absence of significant costs associated with the organization and conduct of space missions. Among the physical differences, we note that the technique of space measurements is associated with the International Celestial Reference System (ICRS), while measurements of rotation by the Sagnac inertial gyrocompass are based on the International Terrestrial Reference System (ITRS). Detecting relativistic rotation effects requires comparing the results of simultaneous measurements in two reference frames. For clarification, we discuss the physics of GR rotational effects in more detail.

5.2.1 Gravimagnetism phenomenon. Gravimagnetism (GM) is a GR phenomenon associated with the presence of mass currents (currents of matter) in the reference frame of the observer, which is assumed to be geocentric and nonrotating. In the case of celestial bodies, including Earth, gravimagnetic effects are associated with the absolute rotation of massive sources of relatively distant celestial objects, quasars. When Einstein's equations in a vacuum are applied to this type of symmetry and linearized, the gravimagnetism effect looks similar to the effect of the magnetic field of a rotating spherical electric charge in electrodynamics. Formally, in the lowest order in relativistic corrections, this effect is described by a dipole gravimagnetic field $\mathbf{B}_{\mathrm{GM}}$ with the dimension of angular velocity. Its explicit form in a nonrotating reference frame centered at the source (in our case, at the center of Earth) is described by the formula (see, e.g., [7, 15, 61])

$$\mathbf{B}_{\mathrm{GM}} = \frac{2G}{c^2 R^3}\left[\mathbf{J}_{\mathrm{E}} - 3(\mathbf{J}_{\mathrm{E}}\mathbf{u}_{\mathrm{r}})\mathbf{u}_{\mathrm{r}}\right], \tag{5.1}$$

where $\mathbf{R} = R\mathbf{u}_{\mathrm{r}}$ is the position vector of the laboratory relative to the center of Earth and $\mathbf{J}_{\mathrm{E}}$ is Earth's angular momentum, whose modulus is the moment of inertia times the angular velocity of Earth.

The influence of field (5.1) on a test body moving with a velocity $\mathbf{v}$ is represented as the effect exerted by a magnetic field on a moving charge in electrodynamics: in fact, the geodesic equation in the weak-field approximation has the form

$$\frac{\mathrm{d}\mathbf{v}}{\mathrm{d}t} = \mathbf{D}_{\mathrm{GE}} + [\mathbf{v}\,\mathbf{B}_{\mathrm{GM}}], \tag{5.2}$$

where $\mathbf{D}_{\mathrm{GE}} = (GM/R^2)\mathbf{u}_{\mathrm{r}}$ is the Newtonian gravitational field.

Thus, the overall effect can be described in terms of a 'gravimagnetic' Lorentz force and a Newtonian force, which can be interpreted as the action of a 'gravielectric' field $\mathbf{D}_{\mathrm{GE}}$.

The rotation of the gravitational field source affects the gyroscope located in its vicinity, and therefore the gyroscope undergoes so-called LT precession, or 'frame dragging' in terms of the reference frame determined by the gyroscope axis [15, 49, 61]. The frame dragging phenomenon also arises for a freely falling test body with zero local angular momentum: a remote observer perceives it as a rotating body in the reference frame of fixed stars [61, 62]. We note that in treating gravimagnetism as an analogue of electromagnetism, a mechanical gyroscope is analogous to a small magnetic dipole (or current loop). Accordingly, the gyroscope behaves in the same way as magnetic dipoles do in an external magnetic field: it precesses.

The equation for the precession of a gyroscope (top) with spin $\mathbf{S}$ moving along a geodesic in the field of a rotating spherical mass is approximately written as [15, 61]

$$\frac{\mathrm{d}\mathbf{S}}{\mathrm{d}t} = \left[\mathbf{\Omega}^*\mathbf{S}\right], \quad \mathbf{\Omega}^* \approx \mathbf{\Omega}_{\mathrm{g}} + \mathbf{\Omega}_{\mathrm{LT}}, \tag{5.3}$$

where the angular precession rate $\mathbf{\Omega}^*$ is determined by two main contributions: the geodesic (or de Sitter) precession $\mathbf{\Omega}_{\mathrm{g}}$ and the LT precession $\mathbf{\Omega}_{\mathrm{LT}}$. The gravimagnetic field of the massive source, $\mathbf{B}_{\mathrm{GM}}$, manifests itself as a relativistic correction to its angular velocity [7, 15, 49, 61]:

$$\Delta\mathbf{\Omega} = -\frac{1}{2}\,\mathbf{B}_{\mathrm{GM}}. \tag{5.4}$$

This important result means that the gravimagnetic GR effect can in principle be detected by a ground-based device, a large-scale ring laser gyroscope [7, 63–65].

Based on the experience with large-size gyrolasers (see Section 3.3), it is reasonable to assume a sensitivity of 10^{-11} rad s^{-1} Hz$^{-1/2}$ is attainable. In principle, this resolution is sufficient (after three months of data collection) to measure the dragging effect of a local reference frame (or the LT effect) with an accuracy of several percent.

5.2.2 Calculation method and numerical estimates. We briefly remark on the method for calculating the frequency of Sagnac splitting due to the phenomenon of gravimagnetism. For this, not only the kinematic effect of laboratory rotation but also the change in the gravitational field due to the rotation of the source must be taken into account (details can be found in [7, 61, 65]).

In GR, if the source of a gravitational field (curvature of space) is a freely rotating mass, the interval $\mathrm{d}s^2$ contains off-diagonal metric components $g_{0\nu}$. In spherical coordinates with the origin at the center of the mass assumed to be in free fall with the radial coordinate r, we let θ denote the latitude angle measured from the axis of rotation of the source, and φ denote the longitude measured from a fixed

direction (relative to fixed stars in space); time t is measured by a chronometer in a remote area where the field is absent. Due to the symmetry in φ, the metric tensor components $g_{\mu\nu}$ depend only on r and θ. The coordinate time interval $\mathrm{d}t$ along the world line of a light beam is found from the condition $\mathrm{d}s^2 = 0$. When light propagates along a closed contour, integration along the propagation path in the right (clockwise, $\mathrm{d}\varphi < 0$) and left (counterclockwise, $\mathrm{d}\varphi > 0$) directions gives different results due to the off-diagonal $g_{0\varphi}$ component of the metric tensor, which changes sign. The difference between travel times in the forward, t_+, and reversed, t_-, directions is

$$\delta t = t_+ - t_- = -\frac{2}{c}\int \frac{g_{0\varphi}}{g_{00}}\, r\sin\theta\,\mathrm{d}\varphi\,. \tag{5.5}$$

The detector at the meeting point of the light waves then records the proper-time difference τ:

$$\delta\tau = -\frac{2}{c}\sqrt{g_{00}}\int \frac{g_{0\varphi}}{g_{00}}\, r\sin\theta\,\mathrm{d}\varphi\,, \tag{5.6}$$

which can be measured by considering the interference of two oppositely rotating beams. The difference between proper times is converted into a difference between the eigenfrequencies of counter-propagating waves, giving rise to the principal characteristic of the optical Sagnac gyroscope, the mode splitting frequency δf_{Sagn} (or the beat frequency of the counter-propagating waves f_{b}). The beat frequency can be measured by analyzing the power spectrum of the signal extracted at some arbitrary point in the ring. The formula for the beat frequency is

$$f_{\mathrm{b}} = c^2\,\frac{\delta\tau}{P\lambda} = -\frac{c}{P\lambda}\sqrt{g_{00}}\int \frac{g_{0\varphi}}{g_{00}}\, r\sin\theta\,\mathrm{d}\varphi\,. \tag{5.7}$$

Substituting the metric elements calculated in the first order of the parameterized post-Newtonian (PPN) formalism in (5.7) leads to a formula for the frequency splitting of the gyrolaser modes (beat frequency) [7, 65],

$$\delta f_{\mathrm{Sagn}} \approx \frac{4\mathbf{A\Omega}}{P\lambda}\,\mathbf{n}_\Omega\mathbf{n}_{\mathrm{G}} + \frac{cJ_\oplus}{R_{\mathrm{E}}^3}\left(\mathbf{n}_r\mathbf{n}_{\mathrm{G}}\cos\theta + \mathbf{n}_\theta\mathbf{n}_{\mathrm{G}}\sin\theta\right), \tag{5.8}$$

where $J_\oplus$ is the angular momentum, R_{E} is the radius of Earth, $\mathbf{n}_{\mathrm{G}}$ is the normal to the plane of the laser gyroscope, $\mathbf{n}_\Omega$ is the vector of its rotation axis, $\mathbf{n}_r$ and $\mathbf{n}_\theta$ are the direction vectors of the geocentric coordinate system, and θ is the latitude of the gyrolaser location. Substituting the terrestrial parameters into (5.8), we obtain the value of the relativistic LT correction to the Sagnac frequency splitting. By order of magnitude,

$$\delta f_{\mathrm{Sagn}} = \frac{cJ_\oplus}{R_{\mathrm{E}}^3} \approx \frac{r_{\mathrm{g}}}{R_{\mathrm{E}}}\,\Omega \sim 10^{-9}\times 7\times 10^{-5} = 7\times 10^{-14}\ \mathrm{rad\ s^{-1}}, \tag{5.9}$$

where r_{g} is Earth's gravitational radius. With the sensitivity of 10^{-11} rad s^{-1} Hz$^{-1/2}$ specified in Section 3.3, the shift in (5.9) can, in principle, be detected with an accuracy of several percent over the measurement time $\tau = 10^7$ s (three months). A more rigorous calculation in [7] predicts the result of measuring the LT effect with an accuracy of 1% over two years of continuous observations.

5.3 Underground installations

An installation consisting of a set of N gyrolasers, sufficiently well isolated from vibrations of Earth's crust in an underground location, can measure the rotational motion of the laboratory relative to the local inertial frame of reference with the accuracy discussed in Section 5.2.2. This measurement is to be compared with the VLBI data on the rotational motion of the 'solid Earth' relative to the system of 'fixed stars.' The difference between the two data sets should allow identifying the small contribution of the LT correction (the method exhibits similarities to the GP-B space experiment [50]).

The laboratory reference frame is not inertial, because it rotates along with Earth. In addition, it is subject to a number of perturbations of various natures (kinematical, geodesic, geophysical, cosmological, and so on). These perturbations are usually several orders of magnitude larger than the magnitude of the LT effect. A thorough analysis of all coherent disturbances is required using measurement data from several ground-based gyroscopes. One laser gyroscope measures the projection of the angular velocity vector on the normal to the plane on which it is located. To obtain complete information about the rotational motion vector, a set of at least three independent gyrolasers is required.

It is obvious that the problem of optimal joint processing of their data arises. Various possible strategies for combining outputs from N rigidly coupled instruments must be explored. A suitable definition must be given for invariant observables (or 'optimal variables') used to compare with VLBI data. It is clear that large-size gyrolasers on a scale of about 6 m are too large to be built into a monolithic structure; heterolithic structures have to be used. The sacrificed mechanical rigidity should be replaced by complex systems of automatic control (maintenance) of linear dimensions. Comprehensive preliminary modeling is required for all effects that can lead to parasitic variations in the output signal, for example, due to changes in geometry, the active optical medium, external perturbations, and so on. Information on practical steps to implement such a program can be found in [7, 65, 66].

Currently, the GINGER (Gyroscopes IN GENeral Relativity) ring laser facility is being created at the Gran Sasso underground observatory (Laboratori Nazionali del Gran Sasso, LNGS) (Italy). This is one of the key projects of the Italian National Institute of Nuclear Physics (Istituto Nazionale di Fisica Nucleare, INFN), implemented in collaboration with the National Institute of Geophysics and Volcanology (Istituto Nazionale Geofisica e Vulcanologia, INGV) in international cooperation with Germany (Technical University of Munich) and New Zealand (University of Canterbury) [67].

The LNGS observatory provides good screening from all types of surface perturbations (the adit depth is 1400 m) (Fig. 14). At the current stage, a square vertical gyroscope with a scale of 3.6 m, representing an intermediate stage called GINGERino [68], has been mounted in the shaft of picket B (arrow on Fig. 14), as far as possible from the activity zone of scientific and technical personnel. This preliminary tool is designed to measure the background of very-low-frequency rotational perturbations inside the LNGS in order to test the suitability of this location for the installation of a large GINGER facility for detecting the relativistic LT effect [69].

A possible GINGER configuration is shown in Fig. 15. The heterolithic octahedral structure is the most compact and, in principle, the simplest in terms of controlling the entire installation. With two octahedra, three closed mutually

Figure 14. (Color online.) Gran Sasso Underground Observatory (LNGS, Italy).

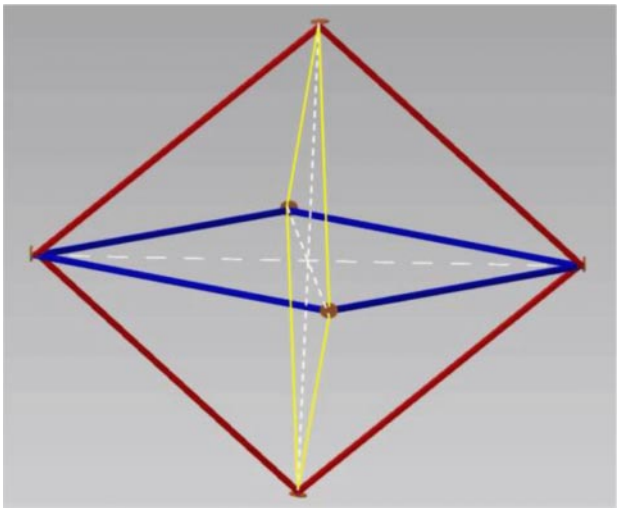

Figure 15. (Color online.) Octahedral configuration of three SGs. Six mirrors form three mutually perpendicular square contours. The geometry is actively controlled by laser cavities installed along three diagonals connecting the mirrors.

orthogonal square contours with adjacent sides (red, yellow, and blue squares) are formed in this structure. The side of each of the three square loops must be at least 6 m. A total of six mirrors are involved in making up three laser gyroscopes. Active geometry control (structural rigidity) and optical control can be achieved using Fabry–Perot (FP) laser cavities as error signal sensors, mounted along three diagonals connecting the vertices of the squares. The geometric accuracy of holding the entire structure, according to the plan, should be at the level of 10^{-10}.

The reference point for the GINGER project is the sensitivity level of the large optical gyroscope GRL in Wettzell. Careful work to control its cavity length and laser discharge parameters has already allowed achieving stability characteristics very close to the photon noise limit, with an integration time of the order of 10^4 s. This corresponds to a statistical error in angular velocity estimates at the level of $10^{-8}\Omega_{\mathrm{E}}$, which is about five times greater than Ω_{LT}, the contribution of the LT effect to Earth's rotation. There are several ways to suppress excess noise a GRL. An obvious resource is to increase the optical power circulating in the ring. In ring lasers with an active medium and self-generation, this power is extremely low ($\sim 10^{-8} - 10^{-7}$ W), but it can be increased by several orders of magnitude when using SG models with external pumping. The technique of a passive ring gyrolaser is not as well developed as that of an active one, but the transition to such SG models for precision experiments is not too remote a perspective.

We note that ground-based measurements of the LT effect are complicated not only by its smallness but also by the fact that it is static in the proposed measuring scheme. Another serious problem is to separate the useful signal from systematic errors of an optical, thermodynamic, and mechanical nature. To eliminate these errors, it would be useful to compare the data obtained at different remote stations with the same instrument. This would facilitate the task of filtering global variations from instrumental and local perturbations. So far, only one more large ring laser, located in Christchurch, is in store, assuming that it will be launched with sufficiently high resolution and stability [5, 66]. In this regard, the creation of a similar facility in underground conditions at the Baksan Neutrino Observatory, Institute for Nuclear Research, Russian Academy of Sciences (BNO INR RAS), analogous to LNGS in Italy, seems to be in high demand. The presence of several global observatories with large gyrolasers would also contribute to the solution to the fundamental astrometric problem of establishing a connection between the local geocentric reference frame and the celestial frame of very distant 'stationary objects' (quasars).

6. Search for dark-matter particles

Applications of ring gyrolasers are not limited to the field of gravity-inertial measurements. As optical interferometers, ring gyrolasers can be used to detect small variations in the refractive index of the medium that fills the optical path. If a light guide is void, then we can talk about quantum fluctuations of the vacuum refractive index (QED effects). In view of the extreme smallness of such effects, a high sensitivity of ring lasers is in demand. There are known proposals for the use of ring gyrolasers in the problem of searching for hypothetical particles of dark matter, axions [3, 9, 10].

6.1 Dark matter problem and axions

Let us recall that modern cosmology is satisfactorily described by a classical solution to Einstein's equations for gravity representing a homogeneous expanding Universe. It is assumed, however, that there is a background of primordial spacetime inhomogeneities due to quantum fluctuations during the exponential expansion phase (so-called inflation). To complete such a description, a number of ingredients are still missing — those that are not in the Standard Model (SM) of elementary particles. In particular, there is dark matter (DM), a substance that under the action of gravity behaves like a cold gas of nonbaryonic weakly interacting particles. By now, it has been proven that most DM is not in the form of neutrinos or some other SM particle.

The axion is a hypothetical spin-zero particle of quantum chromodynamics (QCD), proposed by Peccei and Quinn [70, 71] to solve the so-called parity violation problem (*CP* symmetry) in strong interactions. The axion was further identified by Weinberg [72] and Wilczek [73] as a Nambu–Goldstone pseudoboson of a new spontaneously broken global symmetry, which was actually postulated by Peccei and Quinn (PQ symmetry). It turned out that axions are excellent candidates for the role of DM particles, because they interact very weakly with the environment. Their main production modes in the early Universe are nonthermal and are related to the mechanisms of vacuum reconstruction [74–76] or the decay of topological defects such as strings and domain walls [77–80]. Due to this, axions are produced with an extremely small velocity dispersion and, being cold DM, ideally meet the requirements of the ΛCDM model, which well describes the large-scale structure of the Universe.

Experiments to search for the DM substance (to resolve the DM mystery) have been underway since the early 1990s on accelerators, underground installations, and astronomical instruments in attempts to generate and detect particles of a new type, primarily axions. In the conceptual work of Sikivie [81, 82], two main search methods were formulated: the use of an axion haloscope to detect cosmic axions from the Galactic halo and an axion helioscope to detect the flux of axions emitted by the Sun. These proposals are underlain by natural ideas: (a) the use of efficient natural sources of axions, the Sun and the Big Bang, instead of trying to generate them in the laboratory; (b) the use of coherent effects of signal accumulation at macroscopic distances and long times to increase the sensitivity to their detection.

Experimental activities to implement this proposal continue to this day. Pioneering efforts in the 1990s led to the formation of the Brookhaven–Rochester–Fermilab collaboration, which created the first haloscope [83, 84] and helioscope [85, 86] with moderate sensitivity. A concept of an axion haloscope was implemented in Florida [87], which later became part of the ADMX (Axion Dark Matter eXperiment) setups [88]. The competing CARRACK (Cosmic Axion Research with Rydberg Atoms in a Cavity at Kyoto) haloscope [89] and Tokyo helioscope [90] were built in Japan. Finally, at the end of the 20th century, the CAST (CERN Axion Solar Telescope) helioscope was launched at CERN [91].

6.2 Installations for the search for axion-like particles

Almost all haloscopes share a similar design. Their main goal is to register galactic axions with a low mass ($\leqslant 10^{-5}$ eV) representing cold DM (CDM). We explain the principle of operation of installations with the example of the ADMX complex in the US [88, 92, 93]. The detector is a radio frequency (RF) microwave cavity surrounded by a solenoid and cooled to liquid helium temperature. In the magnetic field of a solenoid (up to 7–9 T), the decay of a galactic axion can generate radio emission in the frequency range of 0.5–1.5 GHz, depending on its mass. Due to the weakness of the effect, only resonant photons are recorded.

Helioscopes search for heavier solar axions with predicted masses up to $10^{-2}-10^{-4}$ eV. The best-known representative of helioscopes of this type is the CAST mentioned in Section 6.1 [91, 94, 95]. The CAST helioscope is a 10-meter dipole magnet with a 9-T field (originally made for the Large Hadron Collider (LHC)) with two straight tubes mounted on a platform movable vertically by $\pm 8^\circ$ to allow observing the Sun for two hours at both sunrise and sunset. The horizontal angular range of $\pm 40^\circ$ covers almost the full azimuthal motion of the Sun throughout the year. In the conversion of axions inside the magnet, X-ray photons are formed. This radiation, after being amplified about 100-fold by focusing X-ray telescopes, is directed to a grating of low-background, low-threshold X-ray detectors.

Installations of both types have been operating for more than 10 years, gradually improving estimates of the upper bounds for the mass and the coupling constant of the axion field. The best current bound on the coupling constant obtained in CAST measurements is $g_a \sim 10^{-10}$ GeV^{-1} [91]. This level corresponds to the limit capabilities of this instrument. However, observations with it continue within the program for searching for other axion-like particles (ALPs) [96, 97]. Numerical diagrams bounding the coupling constants and masses of ALPs are given in a recent publication [98] and on websites [92, 94].

Another direction of the search for axions that is also being actively developed does not require the presence of sources in nature: this is a scheme in which an artificially created source (generator) is placed in a laboratory and the detector installation is located at some distance from it (an analogy with the discovery of EM radiation in Hertz's classical experiments is to be noted). However, a special feature involved here allows referring to this type of experiment as Light-Shining-through-the-Wall (LSW). The general principle is as follows: optical radiation generates a flux of axions (generation) in a strong magnetic field, but cannot penetrate an absorbing screen. The screen is easily penetrated by axions, which then produce new photons in the magnetic field on the other side of the screen. A description of LSW-type setups can be found in [99–102]. We explain their typical configuration with the example of a domestic project presented in [103].

The authors of [103] analyze the RF setup shown in Fig. 16. Two coaxial cylindrical EM cavities are separated by a screening plate of width Δ. The cavities are supposed to have superconducting walls to ensure a sufficiently high quality factor. The generating cavity R_1 can operate in two modes: filled either with resonant RF radiation and a

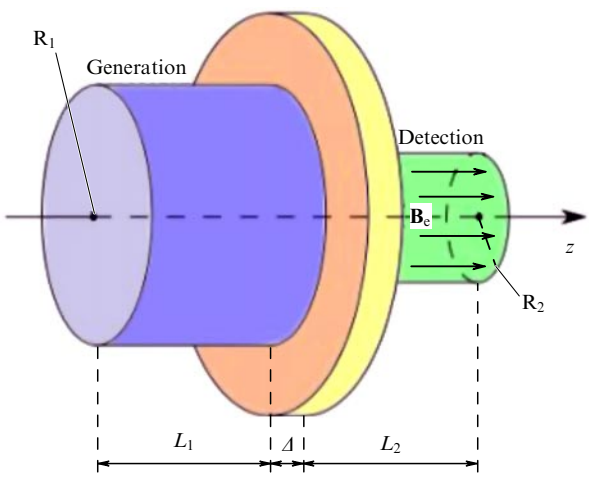

Figure 16. (Color online.) Schematic diagram of an LSW-type installation. Detection cavity R_2 is separated from axion generation cavity R_1 by a screening plate (wall) of width Δ. Both cavities are filled with a constant magnetic field. The generation cavity, in addition, has resonant high-frequency EM pumping.

constant magnetic field (a classic combination for LSW systems) or only with RF radiation, but in no fewer than two modes (such that the EM invariant **EB** is nonzero). Cavity R_2 is filled only with a magnetic field. Under the action of axions that have passed through the screen from the R_1 generator, resonant radio emission is produced in it, which is then detected. In [103], a calculation was made to optimize the parameters of the facility, with the discords between the amplitudes of RF radiation and the constant magnetic field B for superconducting cavities taken into account, along with calculations of the spatial distribution of the generated axion field with a specific geometric form factor. As a result, substituting the optimized parameters in the calculation formulas has shown that sensitivity to the axion–photon coupling constant can be improved by an order of magnitude (to $g_{a\gamma\gamma} \sim 10^{-11}$ GeV^{-1}) compared to the sensitivity in existing installations. The range of tested axion masses can be tuned by selecting the frequencies of the RF modes used. A similar approach was adopted in [101, 102].

We herewith conclude our brief presentation of the DM problem and turn to the main topic of this section, the possibility of detecting axions using ring Sagnac interferometers. We only note that an exhaustive review on the search for ALPs, WIMPs (weakly interacting massive particles), and WISPs (weakly interacting slim particles) is available in [104]; we additionally recommend [105] and lectures [106]. The reader interested in a popular-science presentation can refer to [107].

6.3 Search for dark matter using ring lasers

As an optical interferometer, a large-size ring SG should be suitable for detecting small changes in the refractive index n of the medium filling the optical path. If the light guide is empty, we can speak about quantum fluctuations of the vacuum refractive index (a nonlinear QED effect). However, in the presence of a strong magnetic field and intense optical illumination, other mechanisms of variations δn appear, associated with the generation of axions and ALPs.

The first publication in which a ring SG was proposed as a tool in the search for axions based on the Primakoff effect is apparently [9], which we analyze below. We note before proceeding that both the theoretical basis and the instrumental technique of such a search are very similar to those used in experiments on studying the properties of the vacuum in QED.

Experimental proof of the existence of vacuum quantum fluctuations is based, in particular, on the Casimir effect, the appearance of an attractive force between plates of a planar capacitor caused by the difference between the light pressures of vacuum photons inside and outside the capacitor due to the mode selection of the EM field [108–111]. When the gap between the plates is smaller than 1 μm, the 'vacuum force of attraction' already starts exceeding the Newtonian force [112]. In the presence of a magnetic field, the Primakoff effect also allows explaining the emergence of optical properties of the vacuum. A photon with a suitable polarization in a magnetic field can be converted into an axion and disappear from the observer. The vacuum, as it were, absorbs some of the light with a certain polarization (the one parallel to the magnetic field). This phenomenon is called *vacuum dichroism* or *selective absorption of light*, depending on the polarization. The transformation of a photon into a virtual axion and vice versa leads to a decrease in the phase velocity of the EM wave. Indeed, in the domain of the magnetic field, the beam components of different polarizations travel at different speeds, and the beam splits. This effect is called *vacuum birefringence*. Both effects are extremely small. However, attempts to experimentally register them have been carried out for almost 20 years at one of the INFN research centers, Legnaro National Laboratories (Laboratori Nazionali di Legnaro, LNL) (Ferrara, Italy). The goal of the experiment (and the eponymous collaboration [106]) PVLAS (from Italian Polarizzazione del Vuoto con LASer, vacuum polarization by a laser) is to observe the vacuum polarization that causes a nonlinear optical behavior of laser radiation in magnetic fields [113].

The PVLAS experiments have been ongoing since 2001. The first descriptions and early results are presented in [114, 115]. The detection of a nonlinear 'polarization rotation' effect was reported in [116], but was later discarded as an artifact. After the upgrade of the setup (since 2008), new measurements were made [117–119]. The current level of sensitivity to nonlinear electrodynamic effects in the PVLAS experiment, $A_e < 2.9 \times 10^{-21}$ T^{-2}, is regarded as an upper bound for the factor of nonlinear vacuum perturbations in strong magnetic fields.

We return to study [9], where the first scheme for using large-scale SGs to detect axions was proposed. Additional engineering and technological blocks are introduced into the installation. A mandatory block is a magnet that creates a strong magnetic field in a selected section of the SG contour, which is not directly related to interference with the optical cavity of the gyrolaser. However, additional optical elements that provide rotation of the polarization plane of the light wave have to be placed inside the light path. The beam circulating in the gyrolaser circuit is chosen to be linearly polarized. An external magnetic field defining the 'active zone' is applied to a length-l part of the circuit. There, an optical wave with the vector **E** parallel to the magnetic field **B** effectively produces axions. Phenomenologically, this is reflected by the scalar product of the fields in the interaction Lagrangian $L_a = g_{\gamma\gamma a}(\mathbf{E}\,\mathbf{B})a$, where $g_{\gamma\gamma a}$ is the coupling constant and a is the axion field amplitude. A wave with $\mathbf{E} \perp \mathbf{B}$ does not interact with the magnetic field. A phase difference between the $\mathbf{E}_{\parallel}$ and $\mathbf{E}_{\perp}$ components appears, which can be measured.

The principle of operation of such an axion detector is explained by a simplified diagram taken from [9], which shows one of the arms of a square contour of the SG (Fig. 17) (we consider the SG version with external optical pumping, assuming that its intensity in the ring can be much

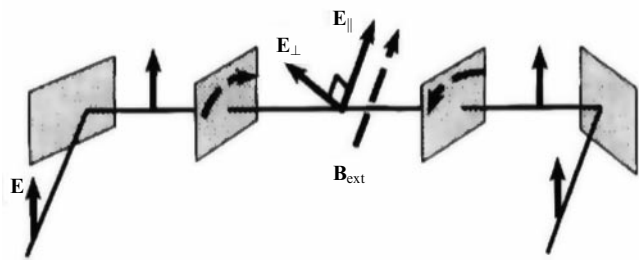

Figure 17. Schematic diagram of axion detector based on a Sagnac ring. Shown is the beam polarization structure in the ring cavity for detecting axions and vacuum QED birefringence. Axion-induced damping and deceleration of the beam polarized parallel to the external magnetic field modulate the output signal of the ring laser.

higher than the 10^{-8} W level typical of self-excited rings). Faraday insulators with opposite directions of optical axes are located at the left and right ends of the active zone containing a magnetic field. They rotate the polarization plane of beams passing through them clockwise and counter-clockwise through a fixed angle (45° in [9]). The polarization of the beams outside the active zone remains unchanged. As a result, only one of the ring waves of the gyrolaser with the vector $\mathbf{E}_{\parallel}$ parallel to the magnetic field can generate axions. The counter-propagating wave, having the vector $\mathbf{E}_{\perp}$ normal to the magnetic field, does not interact with the magnetic field. The phase velocity of the wave involved in the generation of axions decreases, which is equivalent to the appearance of a refractive index not equal to unity. The difference Δn between the refractive indices of counter-propagating waves, acquired in the core, leads to a splitting of the ring modes, which, due to the smallness of the effect, manifests itself as a correction to Sagnac frequency (1.1) due to the rotation of the interferometer. The correction is described by the simple formula

$$\Delta f_{\mathrm{s}} = f\,\Delta n\,\frac{l}{L}\,. \tag{6.1}$$

The following parameters of the installation were used in [9]: gyrolaser size $L = 3.5$ m, active zone length $l = 10$ cm, pump laser frequency of 4.7×10^{14} Hz, and magnetic field amplitude $B = 1$ T. For heavy axions with $m_{\mathrm{a}} \sim 10^{-3}$ eV, this gave an estimate of the equivalent refractive index difference $\Delta n \approx 7.3 \times 10^{-20}$. Using (6.1), we hence deduce the magnitude of the effect: $\Delta f_{\mathrm{s}} \sim 1$ μHz. At the time of writing [9], the authors could rely on the current sensitivity (resolution) of the large G-0 Canterbury gyrolaser, which was $\langle \Omega_f \rangle \sim 11$ prad s^{-1} Hz$^{-1/2}$. Then, using (1.1), we can write the condition for detecting the 'axion splitting' Δf_{s} as

$$\Delta f_{\mathrm{s}}\,\frac{P\lambda}{4A} \geqslant \frac{1}{2\pi}\langle \Omega_f \rangle \tau_{\mathrm{m}}^{-1/2}\,. \tag{6.2}$$

With the above values of the parameters, inequality (6.2) is already satisfied at the measurement times $\tau_{\mathrm{m}} \geqslant 100$ s. But for measurement reliability, a signal-to-noise ratio (SNR) margin of at least one to two orders of magnitude is required.

We note that, in pioneering work [9], only the principle of the experiment on the search for axions with a ring gyrolaser was discussed in order to prove the possibility of attaining a reasonable sensitivity level; the design and optimization of the engineering structure were not mentioned. However, an obvious technical recommendation — the option of a cyclic change in the direction of the magnetic field — was given in [9]. The 'axion effect' would then manifest itself as a weak phase–amplitude modulation of the Sagnac frequency, which, for example, is $\delta f_{\mathrm{s}} = 288$ Hz for the G-0 gyrolaser. The experimental technique will consist in filtering the sidebands of the output signal shifted by the modulation frequency of the magnetic field and measuring their intensity. With a small modulation index ($\sim \Delta f_{\mathrm{s}}/\delta f_{\mathrm{s}} \approx 3 \times 10^{-9}$), this is a very challenging task. Nevertheless, the authors of [9] (1996) conclude with an optimistic forecast regarding the use of large ring lasers to search for DM particles, counting on the progress of this technique in the near future.

Today, it is already clear what actual improvements can be made. Based on the experience of operating the PVLAS facility [106], the vertical design of a square SG would allow increasing the physical length of the active zone with a magnetic field to 1 m (from 10 cm in [9]); the field itself can be increased to 10 T due to the use of superconducting electromagnets in a cylindrical helium cryostat. Finally, the effective path length of the beam in the active zone can be increased due to the use of a multi-reflective delay line on high-reflectivity mirrors (sharpness up to 10^5). We note that the G-0 geodetic gyrolaser had a vertical structure with a side of 3.5 m, being fixed on the Cashmere Cave wall [28]. A calculation of how much the resolution (and sensitivity) of such an upgraded axion detector will be improved has not yet been published.

No detailed information is available in the literature on installations in operation with ring lasers in a magnetic field aimed at searching for ALPs. But ideas and proposals of this type arise periodically. To conclude this section, we discuss the original project presented in recent paper [120] for the detection of ALPs by a dedicated ring laser without the use of a magnetic field.

When analyzing the Cooper–Stedman scheme [9], a 'detection problem' was noted: it is necessary to single out a very small 'axion' mode shift on the background of the dominant splitting (greater by two orders of magnitude) induced by Earth's rotation. In [9], the solution to this problem was associated with synchronous filtering of the sideband signal at the magnetic field modulation frequency. A more radical way out is proposed in the Japanese project [120]: changing the configuration of the lightguide circuit, which, while remaining closed, does not give rise to dynamical mode splitting, or, in other words, has a zero Sagnac effect (the required configuration is obtained if, holding two corners adjacent to one side of the square, we rotate it by 180° without breaking the bonds). The Sagnac effect is nullified because a photon bypassing the contour goes half the way in the direction of the platform (reference frame) rotation, and the other half, against the direction of rotation. The lightguide contour can originally be thought of as not square but rectangular (two long and two short sides), such that the transformed shape of the contour resembles a bow tie. It is visualized in the experimental scheme taken from [120] (Fig. 18). Such an installation can no longer be called a Sagnac gyroscope, but it remains a ring laser cavity. If a magnetic field is created on the horizontal segment of the lightguide by placing the required optical elements in the lightguide, then we arrive at the Cooper–Stedman scheme, in which the dominant signal background of the Sagnac splitting is absent, but small axion mode splitting is preserved.

A special feature of the axion detector proposed in [120] is that no external magnetic field has to be involved. This detector is based on the optical effect of QED: the dependence of the vacuum refractive index on the sense (sign) of the circular polarization of transmitted EM waves in the presence of an axion field.

The principle of operation of the detector in [120] is based on the idea that the axion field of DM, oscillating near the minimum of its potential, creates a small difference between the phase velocities for the left- and right-polarized photons. The theory predicts shifts of resonant modes of counter-propagating light waves that have antisymmetric circular polarizations of the same magnitude but opposite signs. Measuring these shifts is the main goal of the experiment.

The physics of the processes occurring in the setup shown in Fig. 18 is supposed to be as follows. A laser beam, after passing through a $\lambda/4$ plate, acquires circular polarization

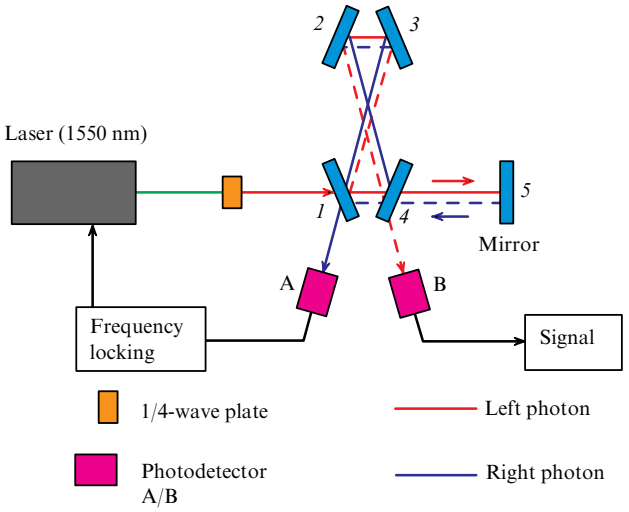

Figure 18. (Color online.) Axion-like particle detector with a modified Sagnac ring. Scheme of an optical bow-tie cavity is shown. Laser beam with left circular polarization is introduced into the cavity from the left. Beam reflected by the far right mirror enters the cavity as a right polarized one. Photodetector A is used to stabilize the laser frequency to the resonance frequency of the clockwise-propagating wave mode. Photodetector B monitors the modulation of the difference between resonance frequencies of the modes of counter-propagating beams.

(say, left-handed for definiteness) and enters the bow-tie cavity. Splitter mirrors *1* and *4* are considered semitransparent, and mirrors *2* and *3*, as well as the end recirculation mirror *5*, are only reflective.

It is important to remember that a circularly polarized beam changes spin when reflected from a mirror: left-hand polarized light becomes right-hand polarized, and vice versa. For example, a left-hand polarized laser beam entering the cavity from the left, upon reflection from mirror *4*, propagates with right-hand polarization to mirror *2*, and so forth. The right-hand polarized beam reflected from the recirculation mirror enters the cavity from the right, but, directed by mirror *1*, becomes left-polarized. We note that, due to the vertically elongated shape of the bow-tie cavity, i.e., along the normal to the laser radiation (see Fig. 18), the beam that enters the cavity from the left is right-polarized for most of its stay in the cavity, and the beam that enters from the right is left-polarized. Thus, the beams that go around the cavity clockwise and counterclockwise have inverse circular polarizations.

As a result, the left beam hits photodetector A and, being reflected from splitting mirror *1*, goes around the entire cavity clockwise. A part of this beam is also transmitted to recirculation mirror *5*. The beam reflected from the recirculation mirror is immediately partially diverted by splitting mirror *4* to photodetector B and then enters it, circumventing the entire circuit in a clockwise direction. From each of these detectors, it is possible to extract the 'error signal' proportional to the difference between the frequencies of the laser and the resonant mode (left or right). It is assumed in this project that the error signal from detector A is used to lock (stabilize) the laser frequency to the mode of the right-hand polarized beam (for example, using the plesiochronous digital hierarchy (PDH) method [121]). The second error signal from detector B turns out to be proportional to the difference between the resonance frequencies of the left and right modes, i.e., the information signal of the experiment.

Without phase velocity modulation $\delta v_{\rm ph}$ due to axion DM, the resonance frequency of the modes would be independent of their circular polarization. Thus, an attempt to find this dependence places the measurements with this setup among the so-called null experiments. It is assumed that the field of galactic axions fills our space, and we try to detect it by the influence of axions on the behavior of photons in cavities. If this effect is not detected in the experiment, then the upper bound of the axion–photon coupling constant is set depending on the assumed mass of the axion.

The expected magnitude of this effect was calculated in [120] using QED tools. But simple approximate estimates can already be obtained phenomenologically, at the physical level of understanding the process. The amplitudes $A^{\pm}$ of the counter-polarized EM modes in the lightguide cavity must obviously satisfy the oscillator equation

$$\frac{{\rm d}^2 A^{\pm}}{{\rm d}t^2} + \omega_{\pm}^2 A^{\pm} = 0\,, \tag{6.3}$$

where the eigenfrequencies of the modes of opposite polarizations are different due to the difference between phase velocities arising under the action of the axion field. This can also be represented phenomenologically as a harmonic oscillation with a frequency depending on the axion mass $m_{\rm a}$,

$$a(t) = a_0 \sin\left(m_{\rm a} t + \delta_{\rm a}\right). \tag{6.4}$$

Then, the mode eigenfrequencies can be expressed as (with k denoting the wave EM vector — the photon momentum)

$$\omega_{\pm}^2 = k^2 \left[1 \pm g_{\rm a\gamma} \frac{a_0 m_{\rm a}}{k} \sin\left(m_{\rm a} t + \delta_{\rm a}\right)\right]. \tag{6.5}$$

Formulas (6.3)–(6.5) are written in the energy system of units accepted in nuclear physics (i.e., in terms electronvolts, with $\hbar = 1$ and $c = 1$). It can be seen that the mode amplitudes $A^{\pm}$ satisfy a parametric equation in which the varying parameter is the phase velocity of counter-polarized waves, $v_{\rm ph\pm} = \omega_{\pm}/k$, $\delta v_{\rm ph} \equiv |v_{\rm ph+} - v_{\rm ph-}|$, whence we finally find

$$\delta v_{\rm ph} \simeq \frac{g_{\rm a\gamma} a_0 m_{\rm a}}{k} \sin\left(m_{\rm a} t + \delta_{\rm a}\right) \equiv \delta v_{\rm ph\,0} \sin\left(m_{\rm a} t + \delta_{\rm a}\right). \tag{6.6}$$

For laser light with wavelength $\lambda = 2\pi/k = 1550$ nm, we obtain the estimate

$$\delta v_{\rm ph\,0} \simeq 3 \times 10^{-24} \frac{g_{\rm a\gamma}}{10^{-12}\ {\rm GeV}^{-1}}\,, \tag{6.7}$$

where we used the current value of the upper bound for the axion DM energy density $\rho_{\rm a} = m_{\rm a}^2 a_0^2/2 \simeq 0.3$ GeV cm^{-3} [104].

The possibility of detecting such variations in phase velocity is estimated by the authors of [120] only on the background of quantum photon noise, invoking the fact that mirror jitter noise is compensated in the difference scheme (see Fig. 18) of counter-propagating waves going around the same mirrors. This also applies to the mechanical 'back reaction' effect — stochastic jitter of the mirrors under the action of light pressure. Moreover, the radiation power inside the lightguide reaches several hundred watts, which is ten orders of magnitude higher than for self-pumping ring lasers. As a result, it is predicted that installations of this type (with a lightguide size of 1 m and light power of 100 W) will allow achieving the following resolution in terms of axion field

parameters: $g_{a\gamma} \leqslant 10^{-12}$ GeV^{-1} for the coupling constant and $m_a \sim (10^{-13} - 10^{-16})$ for the masses.

6.4 Experiments at the Baksan Neutrino Observatory

In Section 5.3, we noted the desirability of an installation with a Sagnac gyrolaser placed in the underground BNO INR RAS laboratory for independent observation of relativistic gravity effects (such as the LT effect). Measurements in parallel with the GINGER facility at the LNGS (Lacvilla, Italy) would help eliminate a number of local systematic errors. The same can be said about experiments to search for ALPs. Such activity is under way in both laboratories. In particular, the BNO facility has been used for several years to search for monochromatic axions with an energy of 9.4 keV emitted during the M1 transition in ^{83}Kr nuclei on the Sun. On Earth, such axions can be detected in the reverse reaction of resonant absorption, by detecting X-ray quanta and Auger electrons that arise during the relaxation of an excited nuclear level. The experiment involved a large proportional counter filled with krypton (99.9% ^{83}Kr) [122]. The facility was located in the underground low-background BNO INR RAS laboratory at a depth of 4900 meters of water equivalent [123].

As a result, a new bound for the axion–nucleon coupling constant was obtained, $|g_{a\gamma} m_a| \leqslant 6.3 \times 10^{-17}$, which corresponds to the bound for the hadronic axion mass $m_a \leqslant 12.7$ eV at a confidence level of 95% [124].

We note that the technique of this experiment is associated with a high spectral energy selectivity in the absence of any modulation of the effect with respect to the time of day, which reduces its effective sensitivity. The use of search schemes involving ring gyrolasers of the type considered in [120] would ensure a more broadband reception. The detection probability noticeably increases according to models that predict the modulation of the concentration of galactic axions during the orbital motion of Earth.

7. Tests of GR with combined detectors

In Section 5, we discussed the applications of SGs for detecting the LT relativistic gravitational effect. This is not the only possibility of using ring lasers in testing GR predictions. In Sections 7.1–7.3, we show how such setups can be used, on the one hand, for experimental tests of the foundations of GR, including the equivalence principle (EP), and, on the other hand, for studying one of the fundamental consequences of GR, the existence of gravitational waves (GWs).

7.1 Search for violations of Lorentz invariance with Sagnac rings

Lorentz invariance is at the base of both the SM of particle physics and GR [15, 59, 125–127]. In SR, this is the statement that physical laws are the same in inertial frames of reference, the transition between which is described by Lorentz transformations (translations and rotations or Lorentz boosts). In GR, this principle is formulated as local Lorentz invariance (LLI) for regions in which the gravitational field can be compensated by inertial fields [15, 59]. Thus, LLI is one of the manifestations of the EP that physical laws are independent of the velocity of a reference frame.

In the SM of particle physics, a Lorentzian boost is understood in a generalized form, including the parity transformation of wave functions [127–129]. Attempts to reconcile the concepts of Lorentz invariance in the SM and GR lead to ideas that LI is only an approximation at currently attainable energies [128, 129]. A number of quantum gravity effects are associated with LI violation, which has stimulated a significant number of theoretical and experimental studies in recent decades [130–135], including on the search for LI violations using optical ring cavities. This toolkit turns out to be convenient for studying LI violations under parity transformations. The fact is that circularly polarized counter-propagating light waves in the ring of a gyrolaser are mutual mirror reflections, or an 'odd parity' transformation of each other (a transformation with an eigenvalue of -1). Detecting a difference between the propagation velocities of these waves in a medium without dispersion, loss, and birefringence would be a signature of LI violation.

As a specific example, we briefly describe a test experiment with a triangular gyrolaser performed at the University of Tokyo by a group also involved in the development of GW interferometers, the technology that actually underlies LI tests in the optical frequency range [136]. In this experiment, LI violation was tested by comparing the resonance frequencies $\nu_\pm$ of two counterbeams in an annular cavity, which itself could rotate through a given finite angle in the laboratory. The optical cavity of the ring had an elongated triangular structure with mirrors fixed on a dielectric holder, a spicer made of superinvar with through holes for the optical path. One of the sides had a notch to accommodate a piece of silicon that created an optical asymmetry of the path.

According to theory, a ring interferometer is directly sensitive to 'odd parity' parameters only if it is asymmetric [137–139]. A general analysis and calculation of the resonance frequency shift due to LI violation in such a configuration can be found in [129, 134].

The strategy of the experiment in [136] is as follows. The LI violation is sought in the differences between the physical characteristics of the behavior of the parity partner after a generalized Lorentz transformation, in this case, in the differences between the frequencies of counter-rotating circular polarization modes in a lightguide circuit. In practice, these differences reside in the difference between the eigenfrequencies of the polarized modes $\Delta\nu = \nu_+ - \nu_-$. To improve filtering on a noise background and reduce systematic errors, the measurements were carried out in a dynamical mode. Optical and mechanical elements were placed in a vacuum chamber mounted on a turntable controlled by a servomotor. Forward and reverse rotations through 360° were repeated; the rotation speed was $\omega_{\rm rot} = 30^\circ$ s^{-1} ($f_{\rm rot} = 0.083$ Hz).

The final results of these measurements presented in [136] are as follows. The empirical mean amplitudes of the effect at the modulation frequency turned out to be zero. The standard errors of the mean amplitude were $\sim 2 \times 10^{-15}$, which gives an improvement factor of ~ 1.4 over previous results [130]. Deviations from zero by more than 1σ were not detected. This means that there are no signs of anisotropy of the speed of light in the sidereal reference frame at the level of $\Delta c/c \sim 10^{-14}$. Thus, no LI violation in the photon sector was found by the Tokyo group.

7.2 Mixed Sagnac–Michelson interferometers

As this brief review shows, tests of LI violations carried out so far have not required the use of large-scale ring laser interferometers (except tests on accelerators, which we do not consider).

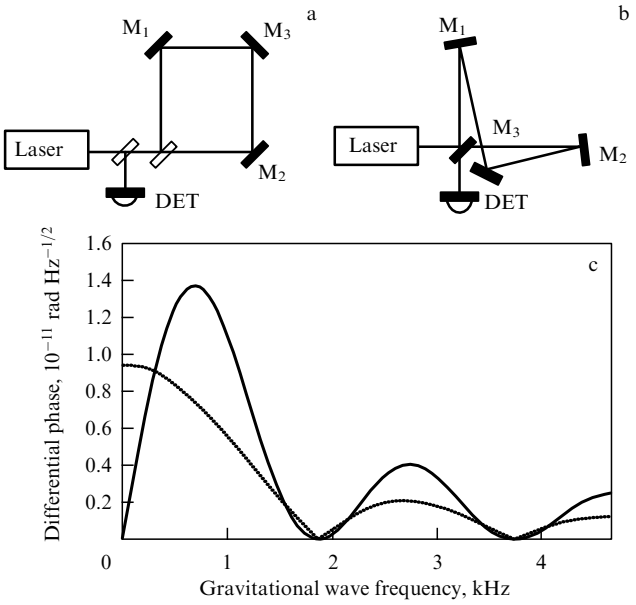

Figure 19. Comparison of interferometers with different topologies. (a) Classical Sagnac interferometer. (b) Combined Sagnac–Michelson interferometer with zero area. (c) Estimated curve of the differential phase — response to a GW signal; response of the Michelson interferometer is shown with the dotted line.

The situation changes dramatically when we turn to elucidating the role played by large-size optical Sagnac rings in the problem of producing a new generation of laser gravitational antennas with a sensitivity that exceeds the standard quantum limit. Such antennas themselves — modern GW interferometers on free-mass mirrors — are gigantic installations with optical arm lengths of several kilometers, and therefore their combination or the introduction of Sagnac configurations with additional mirrors into their designs inevitably leads to industrial-scale installations. In this section and in Section 7.3, we discuss the main motivations and principles for such a combination.

Apparently, the first mention of the possible use of the Sagnac principles in the Michelson design of laser gravitational detectors belongs to their creators, R Weiss and R Driver. In 1986, Weiss proposed an open-type Sagnac interferometer for detecting astrophysical GWs [141]. But, back in 1982, Driver considered (and created a prototype of) a multi-reflective Michelson interferometer with an annular cavity for recirculating beams, with the resonance in the cavity increasing the sensitivity to narrow-band periodic GW signals [142]. However, the first actual study of the combined design of a Sagnac–Michelson interferometer was carried out already in the midst of active work on the creation of the ground-based gravitational antennas LIGO (Laser Interferometer Gravitational-Wave Observatory) and Virgo by a Stanford University group [143].

The authors of [143] consider schemes of ring interferometers shown in Fig. 19. An ordinary Sagnac ring laser with external pumping is shown in Fig. 19a, and its modification — a combined Sagnac–Michelson interferometer with zero effective area — is shown in Fig. 19b. In the modified design, the end mirrors M_1 and M_2 of the Michelson arms are tilted, such that the reflected beams are directed through the splitter to the output of the interferometer with a DET photodetector by means of an auxiliary M_3 mirror along symmetric closed contours, which they pass in opposite directions. Obviously, the area encompassed by the beams (with their direction taken into account) is ideally zero and the usual Sagnac effect due to the rotation of the platform (reference frame) is absent. At the same time, the response of the interferometer to dynamical tidal deformations of the arms induced by the GW is preserved.

In the simplest version, it is assumed that a GW arrives at the detector plane with the + polarization, such that the principal components of the strain tensor lie along the arms of the interferometer. Then, the deformation signals are out of phase (shifted by 180°), and therefore the phases of the counter-propagating (clockwise and counterclockwise) optical waves are related as $\phi_{\rm cw} = -\phi_{\rm ccw}$, and the differential phase is $\Delta\phi = 2\phi_{\rm ccw}$. For one full round trip, the calculation in [140] gives the phase difference modulus

$$|\Delta\phi| = 4 f_{\rm opt}\,\frac{h_{\rm g}}{f_{\rm g}}\,\sin^2(\pi\tau_{\rm s} f_{\rm g})\,, \tag{7.1}$$

where $f_{\rm opt}$ is the laser frequency, $\tau_{\rm s}$ is the accumulation time (of one round trip with attenuation taken into account), $h_{\rm g} \sim (\Delta L/L)$ is the dimensionless GW amplitude (metric variation), and $f_{\rm g}$ is the GW frequency.

A similar formula for the phase difference of interfering beams in the output signal of the Michelson interferometer is

$$|\Delta\phi_{\rm M}| = 2 f_{\rm opt}\,\frac{h_{\rm g}}{f_{\rm g}}\,\left|\sin(\pi\tau_{\rm s} f_{\rm g})\right|\,. \tag{7.2}$$

Formulas (7.1) and (7.2) suggest a clear interpretation of the main characteristics of receiver antennas of two types. In particular, in [140], phase shifts are plotted as functions of $f_{\rm g}$ (Fig. 19c) for the limit of GW signals detectable by LIGO antennas with a spectral density $h_{\rm g} \sim 10^{-22}$ Hz$^{-1/2}$. The other parameters used in the same calculations are as follows: Michelson interferometer arm length $L = 4$ km, optical pumping at $\lambda = 1064$ nm, and sharpness of shoulder cavities of 20 (the number of double passes), whence $\tau_{\rm s} \sim 2(2L/c) \times 20$. The pump power at the beam splitter was assumed to be 5 kW. The conclusions that can be drawn from comparing the plots in Fig. 19c are as follows.

The Michelson interferometer has the highest response at quasistatic frequencies and in secondary reception zones at frequencies determined by the transcendental equation $x = \tan x$, where $x = \pi\tau_{\rm s} f_{\rm g}$. The Sagnac–Michelson interferometer has a maximum response at frequencies defined by the equation $2x = \tan x$. The first and highest peak occurs at $f_{\rm g}^{\max} = 0.37/\tau_{\rm s} = 0.74/t_{\rm loop}$, where $t_{\rm loop}$ is the time to circumvent the Sagnac loop. Setting $\tau_{\rm s}$ in principle allows tuning the frequency corresponding to the maximum to the middle of the GW band. The peak response of the combined interferometer is higher than that of a 'purely Michelson' interferometer due to the greater accumulation of phase when the beams pass through both arms. With the above numerical parameters, the middle of the best reception zone is at $f_{\rm g}^{\max} = 690$ Hz with a width (at a 3 dB level) of approximately 220–1250 Hz. The spectral density of the photon phase noise corresponding to the limit detectable GW is $\sim 10^{-11}$ rad Hz$^{-1/2}$. This, of course, was obtained for interferometers with the specific parameters chosen by the authors of [143], but they are very close to the characteristics of antennas that detected GW bursts from merging relativistic binary stars [144–146].

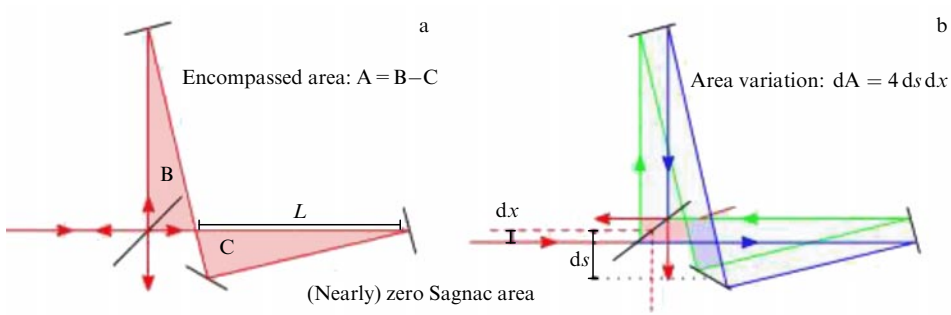

Figure 20. (Color online.) Combined Sagnac–Michelson interferometer. Errors of the combined Sagnac–Michelson scheme. (a) Zero-area Sagnac interferometer; fine tuning of arm length and angles of the end mirrors is assumed; areas B and C highlighted in red are such that the total area encompassed by the beams is equal to zero (taking path direction into account). (b) Changing the encompassed zone under transverse displacements of the beam: a slight change in its position or alignment of interferometer mirrors leads to a change in the area of the encompassed zone; total area A with nonzero mean fluctuates at nonzero frequencies.

But regardless of the quoted values, a qualitative picture of the comparison of traditional and upgraded types of GW laser detectors already reveals the advantages of the latter, prompting their more thorough study. Such advantages, among other things, include reductions in the requirements for frequency fluctuations of optical pumping, seismic perturbations of probe mass mirrors, and systems for their quasistatic mutual positional control.

The authors of pioneering study [143], not restricting themselves to a theoretical analysis of a combined interferometer, conducted test experiments with a table-top model of a new detector, confirming its main expected characteristics. A year later, similar experiments were carried out at the MPI with approximately the same results [147]. However, the question of a new upgrade of GW interferometers quite reasonably arose in connection with the problem of creating the third generation of gravitational detectors within the Einstein Telescope (ET), Voyager, and Explorer projects [148–150].

In the classical Sagnac ring, the phase difference of counter-propagating waves depends on the contour area A and the wavelength λ of the optical pump: $\Delta\varphi = 8\pi\mathbf{A\Omega}/(c\lambda)$. In the upgraded ring with zero area, the leading effect of mode splitting is absent (the Sagnac frequency averages to zero). But fluctuations in the area and in the laser frequency remain among the factors limiting the sensitivity of the combined interferometer as a GW detector. These limitations were estimated in [150] when developing the optimal design for the ET project [148, 149] (Fig. 20).

In the combined configuration, for example, a random angular misalignment of the input beam and mirrors that changes the contour area A can be interpreted as an equivalent change in the laser pumping frequency (additional frequency noise). For the angular mismatch magnitude $\alpha = 10^{-7}$ arc seconds, the calculation of the frequency standard deviation performed in [150] yielded $\Delta\nu \leqslant 1.9 \times 10^8$ (Hz Hz$^{-1/2}$), which is within the permissible errors for the ET project. In this case, a length of the arms $L = 10$ km and level of limit deformation noise $h = 6 \times 10^{-24}$ Hz$^{-1/2}$ were assumed.

Two other channels for excess noise penetration into the combined interferometer are related to seismic factors. First of all, these are seismic perturbations of mirrors, including the rotational component. Assuming the seismic noise of the end and middle mirrors of the combined interferometer to be uncorrelated, the authors of [150] estimated the level of penetrating seismic noise when the input beam is decentered by $\mathrm{d}x = 0.1$ mm (Fig. 20b), which corresponds to the area variation $\Delta A = 0.5$ m^2 (at $L = 10$ km), which in turn predicts the magnitude of uncompensated seismic 'shakeup' of the mirrors at the level of $\Delta\sigma \leqslant 1.8 \times 10^{-7}$ m.

Finally, another consequence of seismic factors is angular input beam jitter. Beam jitter also leads to random variations in the encompassed area, but the mismatch parameter is given here by $\mathrm{d}s$, the distance between the beam splitter and the central turnable mirror (Fig. 20b). For $\mathrm{d}s = 1$ m, the estimate of the seismic effect of jitter also turns out to be quite small: $\Delta\sigma \leqslant 8.3 \times 10^{-8}$ m.

Summarizing the interference analysis [150], we note that satisfying the constraints found for the parameters of the combined interferometer for the next generation of GW antennas is not unfeasible technologically. Most of them have already been implemented in operating free-mass laser detectors. We mean their obligatory unit, a mode filter (mode cleaner), which is a buffer cascade between an optical-pump laser and a multimirror interferometer, which is the GW detector. Such a mode filter is constructed in accordance with a triangular ring scheme, also on suspended mirrors, with all the attributes of seismic and vacuum protection, thermal stabilization, and compensation for backscattering effects. Thus, a solid technological basis for the creation of third-generation GW antennas is currently available.

7.3 Sagnac interferometer in the problem of quantum nondemolition measurements

Until now, the motivation for using a combined Sagnac–Michelson interferometer with a zero equivalent area of the lightguide (as a promising design for a new generation of gravitational antennas) has been the desire to reduce the effect of background noise, of both an external (seismic) and internal (frequency fluctuations of optical pumping) nature. However, it has been realized in recent decades that such a configuration is useful for solving another fundamental problem: overcoming the quantum limits of sensitivity in precision experiments. This problem is of course not limited to the needs of GW detectors. It is relevant both for a wide class of experiments with test bodies and, in principle, for the development of the theory of measurements in quantum mechanics. It is just the GW astronomy that is currently playing the important role of a catalyst for accelerating such research with the ultimate goal of eliminating the apparent agnosticism regarding the problem of limit measurements and reaching practical recommendations.

The main driver of this topic at the end of the twentieth century was the group headed by V B Braginsky at the

Faculty of Physics at Lomonosov Moscow State University: they constantly drew attention to the relevance of the problem and the need to solve it as soon as possible. In fact, all the first studies in this field were carried out entirely by Braginsky's group or with its participation. A natural close collaborator was the California Institute of Technology (USA) group headed by K S Thorne, who at that time was one of the leading proponents of GW astronomy.

7.3.1 Concept of QND measurements. A gravitational antenna provides a particular example of an experiment with test masses whose motion allows the observer to detect and measure the action of gravitational radiation. For this, a parametric converter of mechanical perturbations into an electromagnetic signal — a sensor — is typically used; the sensor can have external RF, microwave, or optical pumping. When mechanical Brownian noise is suppressed by cooling and due to a high quality factor of the detector, the pump quantum noise becomes the main source of fluctuations in the system. Its role is reduced as the pump intensity increases, but then the noise of test masses induced by photon pressure increases (the effect of the back reaction of the sensor on the detector).

As a result, the quantum sensitivity limit of a gravitational antenna arises, determined by the so-called quantum standard or the minimum detectable displacement of test masses: $\sigma_q = [\hbar/(m\omega_\mu)]^{1/2}$ for a resonant Weber antenna and $\sigma_q = [\hbar/(m\tau^{-1})]^{1/2}$ for a laser free-mass antenna. Here, m is the characteristic test mass, ω_μ is the resonance frequency, and τ is the measurement time, of the order of the inverse GW frequency.

Estimates made in pioneering studies [151, 152] (and since then in numerous others) show that, for the typical parameters of the LIGO and Virgo antennas, the quantum sensitivity limit is $\sigma_q \sim 10^{-17} - 10^{-18}$ cm for absolute displacements and $h \sim 10^{-23} - 10^{-24}$ Hz$^{-1/2}$ for deformations in the frequency range of $10^2 - 10^3$ Hz. In [151, 152], possible strategies for overcoming the quantum limit are discussed, associated with a change in the measuring procedure itself. For such a procedure, the term *quantum nondemolition measurement* (QND) was proposed in [151]. The key element of the procedure is the search for a convenient 'quantum-consistent' variable (a QND variable), such that observing its evolution allows accurately measuring the external influence (force). In one of the first papers by Thorne's group [153] on this subject, the model problem of measuring the quadrature components of a quantum oscillator was discussed as a prototype of a resonant gravitational antenna. The authors show the possibility of bypassing quantum restrictions. However, the measurement scheme they proposed was at the level of a thought experiment, i.e., remote from reality.

Another approach was developed in [154], where a system consisting of a test mechanical oscillator with a parametric EM transducer was analyzed from the standpoint of the optimal filtering theory. By that time, a quantum generalization of this theory had been published (see, e.g., [155, 156]). The result of calculations in [154] also demonstrates the possibility of suppressing the quantum limit by taking the correlation between the pump quantum noise and the feedback noise into account. The degree of suppression increases linearly with increasing pump amplitude beyond its QND threshold $C_{\rm opt}$, but the effect is narrowband and spectrally selective.

The problem of QND observables was studied in the general form in [157, 158]. It was shown that integrals of motion of a quantum system are such observables. The operators of these observables commute with each other at different times, and the uncertainty of the initial state reduces to zero as a result of the first quantum measurement. In fact, the commutativity of operators at different times was an important indicator in developing practical QND measurements.

Independently, in [159], for schemes with optical interferometers, attention was drawn to the role of special 'squeezed' quantum states of light in achieving a sensitivity beyond the quantum limit threshold. The idea in [159] was repeatedly used in subsequent papers. In particular, it was taken into account in [160, 161] when designing and calculating the circuit of a resonant GW detector with an FP standard as the detecting sensor (the currently implemented GW detector OGRAN [162]). The result in [160, 161] was proof that a sensitivity exceeding the quantum limit can be achieved when shapers of spectrally selective compression of pump light are included in the setup.

7.3.2 Sagnac ring to measure the speed of mirrors. Laser interferometers based on suspended mirrors in a frequency range noticeably exceeding the pendulum frequency of the suspensions are regarded as GW detectors with free test masses. For a free-mass mirror, its momentum is a quantum mechanical integral of motion. The understanding of this fact stimulated the authors of [163] to seek a QND detector of the state of a test mass as a measure of its speed, i.e., a speed meter (because speed is not identical to momentum, a correction can be made in the course of data processing).

In [163], an example of a speed meter for the angle of rotation of a torsion pendulum having a dielectric rectangular weight holder was considered (see the figure in [163]). Parallel to the weight holder (which is the test mass), a measuring device is placed, which is a fiber lightguide bent into a sinusoid with straight sections at the ends of the weight holder. By varying the wave phase in the lightguide (during wave propagation between straight sections), the average speed of rotation of the weight holder is recorded. The effect of the back reaction of noise of the meter (lightguide) is partially compensated by double (repeated) measurements of the phase in the straight sections at the ends of the weight holder. As much as this compensation allows, it is possible to go beyond the quantum limit for the torsion pendulum sensitivity. An overview of the QND problem and a synthesis of the main ideas shaped by the end of the 20th century can be found in monograph [164].

A new turn in the development of the problem was stimulated entirely by the task of creating GW laser interferometers (broadband GW detectors) of a new (third) generation, reaching and exceeding a sensitivity level of 10^{-24} Hz$^{-1/2}$. Attention was then drawn to the combined Sagnac–Michelson interferometer with a zero lightguide area. The usefulness of such a configuration for the implementation of QND measurements was apparently first mentioned in [165] and somewhat later, with the addition of useful details, in [166, 167]. The schemes of the combined interferometers proposed in these studies are quite similar and on average (qualitatively) correspond to Fig. 21, which allows the physics of the process to be explained.

In order not to overload Fig. 21, the M_3 mirror in the combined interferometer is unified with (or installed parallel

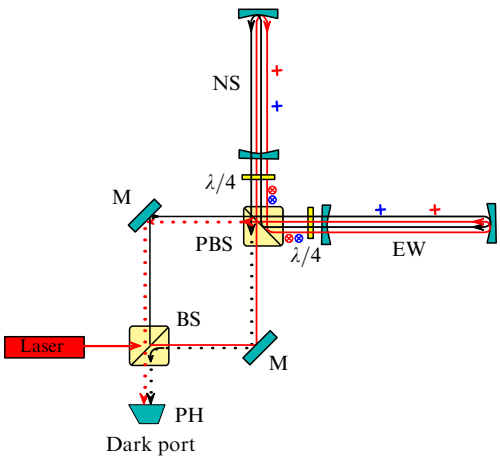

Figure 21. (Color online.) Combined Sagnac–Michelson interferometer as a QND speed meter. NS — north–south arm, BS — beam splitter, PBS — polarization beam splitter, EW — east–west arm, PH — photodetector.

to) the diagonal plane of the polarization beam splitter (PBS). A conventional splitter (BS) splits the pump laser beam into equal parts in terms of power (valve units are omitted); in addition, the PBS also performs polarization selection. For simplicity, we assume that the laser immediately emits radiation polarized in the plane of the drawing, and the PBS lets these beams go straight. $\lambda/4$ plates endow the beams with circular polarization, and the beams circulate in the arm cavities a large number of times (proportional to the FP sharpness). Leaving a cavity, they again pass through a $\lambda/4$ plate, acquiring a polarization perpendicular to that of the incoming beams. The beams of both directions circumvent the total contour made of the two arms of the Sagnac–Michelson interferometer, whose effective area remains zero. As a result, there is no pure Sagnac effect in the interference pattern at the BS, but the signals of the end mirror displacements persist.

It is convenient for what follows to adopt some conventions. The vertical arm in Fig. 21 is called northern, and the horizontal one, western. We let R denote a beam that, after the splitter, enters the interferometer first through the north–south (NS) arm, bypassing it clockwise, and only then enters the second arm. The NS arm parameters are indicated by the subscript N, and the coordinate of the end mirror is denoted by $x_{\mathrm{N}}(t)$. Accordingly, L denotes a beam that, after the splitter, enters the interferometer first through the west–east (WE) arm, bypassing it counterclockwise, and then enters the first, NS, arm. The parameters of the WE arm are indicated by the subscript E, and the coordinate of its end mirror is denoted as $x_{\mathrm{E}}(t)$. It is clear that R and L only indicate the direction of clockwise and counterclockwise rotation of the beam in the first half of the contour.

The result of beam interference at BS (see Fig. 21) was calculated in [166]. The motion of the end mirrors of the two arms produces phase modulation of the pump light, generating sidebands that are filtered by a synchronous detector. Only antisymmetric, nonstatic variations in arm lengths can contribute to the interferometer output signal. The calculation performed in [166] gives the phases of the R and L beams (after passing from the input port through two arms to the output port of 'dark interference') in the form

$$\delta\Phi_{\mathrm{R}} \sim x_{\mathrm{N}}(t) + x_{\mathrm{E}}(t+\tau_{\mathrm{arm}})\,, \quad \delta\Phi_{\mathrm{L}} \sim x_{\mathrm{E}}(t) + x_{\mathrm{N}}(t+\tau_{\mathrm{arm}})\,,$$

where τ_{arm} is the average residence (accumulation) time of light in the arms. The amplitude at the output of the dark port is proportional to the phase difference of the two beams:

$$\delta\Phi_{\mathrm{R}} - \delta\Phi_{\mathrm{L}} \sim \left[x_{\mathrm{N}}(t) - x_{\mathrm{N}}(t+\tau_{\mathrm{arm}})\right] - \left[x_{\mathrm{E}}(t) - x_{\mathrm{E}}(t+\tau_{\mathrm{arm}})\right].$$

Assuming τ_{arm} to be small and expanding in a series, in the first order, we obtain

$$\frac{\delta\Phi_{\mathrm{R}} - \delta\Phi_{\mathrm{L}}}{\tau_{\mathrm{arm}}} \approx \langle v_{\mathrm{N}}\rangle - \langle v_{\mathrm{E}}\rangle\,,$$

where $\langle v_{\mathrm{N}}\rangle$ and $\langle v_{\mathrm{E}}\rangle$ are the average velocities of the end mirrors over time τ_{arm}.

Thus, the combined Sagnac–Michelson interferometer acts here as a QND speed meter, decreasing the quantum mechanical sensitivity limit threshold by a factor $\Omega\tau_{\mathrm{arm}} \ll 1$, where Ω is the GW signal frequency (from the typical range $10^2 - 10^3$ rad s^{-1} for operating GW detectors) [165, 167].

7.3.3 Combined interferometer as a third-generation GW detector. The diagram in Fig. 21 was shown to explain the operation of a combined-topology interferometer as a speed meter for test-mass mirrors. However, the actual design of operating GW interferometers also contains other complicating units. Among these, the so-called recirculation nodes (returning the radiation leaving the interferometer to its circuit) are fundamental: (a) a power recycling mirror (PRM) and (b) a signal recycling mirror (SRM), which are meant to reduce the laser pump power and increase the useful response of the interferometer by means of signal accumulation. This is achieved by adding two more mirrors to the light (input) and dark (output) ports. The idea of recirculation was proposed in [168]. Details of the recirculation schemes are given in the descriptions of the LIGO and Virgo installations [169].

Complete designs of GW detectors with a combined topology (with the possibility of using optical pumping in a quantum squeezed state taken into account) were analyzed in [170, 171] in connection with the ET and Voyager projects [148, 149]. A group at the Faculty of Physics of Moscow State University [170] studied the procedure for optimizing the parameters of interferometers for each of these projects. Using the statistical operation of introducing a penalty (or 'cost') function, a combination was found in the parameter space that provided the maximum suppression of the sum of quantum fluctuations and instrumental noise. The result obtained shows that, in a combined interferometer with light recirculation systems in the pump (input) and signal (output) ports, the predicted sensitivity of GW detectors with the Sagnac–Michelson topology for the ET and Voyager projects must be at the level of $\sim 3 \times 10^{-25}$ Hz$^{-1/2}$ in the received frequency band of $\sim (70-400)$ Hz, which is within the scope of the design specifications.

Concluding this brief description of the role of Sagnac interferometers in the problem of quantum measurements, we note that a complete review of the current state of the problem with an extensive list of references is available in [172]; there, the authors focus on the quantum mechanical form in presenting the material. At the same time, it is known that the classical representation of precision measurements in the language of parametric systems is also possible in radiophysics and optics. Such systems are also characterized by

phase-sensitive, frequency-selective measurements and processes with variables that are each other's antagonists, for example, the quadrature components of a stochastic oscillator. The need to accurately measure (enhance) one of the variables leads to an increase in the error in information about the other (as for noncommuting quantum observables). This point of view is present in the work of Gertsenshtein [173]. In addition, if a quantum description is natural for optical radiation, an analysis of a macroscopic oscillator (in the form of a pendulum or a solid body mode) in quantum terms, even at low temperatures and low dissipation, is not necessary. These issues are discussed in [174], where it is shown that such an oscillator also requires a low-energy state, close to the ground state, to manifest its quantum properties. This was experimentally confirmed at the LIGO facility (Hanford) [175].

8. Sagnac gyroscope on cold atoms

As shown in Section 2, the Sagnac effect is universal with respect to the nature of objects running along the ring, be it harmonic EM waves, solitons, or particles. This is a purely kinematic effect, a consequence of the addition law for velocities in SR. From the quantum mechanical standpoint, the flow of atoms propagating in the Sagnac contour can be regarded as matter waves with a wavelength corresponding to the de Broglie relation $\lambda_{\rm B} = 2\pi\hbar/p$, where $\hbar$ is the reduced Planck's constant and p is the momentum of the atom. For light atoms with masses $m_{\rm a} \sim (1-100)m_{\rm H}$ (where $m_{\rm H}$ is the mass of the hydrogen atom) at thermal speeds, the 'matter wavelength' turns out to be of the order of 10^{-9} m, which is three orders of magnitude less than that of EM waves in the optical range. The resolution and potential sensitivity of interferometric measurements should increase accordingly. Such a physical understanding and obvious advances in the technique of creating a flux of cold atoms rekindled studies of Sagnac rings based on matter waves and their applications to problems in fundamental physics.

In the late 1980s, various types of atomic interferometers were proposed as sensitive probes for various physical effects [176–178]. By the early 1990s, the first experimental setups appeared [179–182]. The predictions of a high sensitivity of atomic interferometers (to inertial effects in particular) were confirmed. At present, atomic interferometers are used in leading laboratories as precision instruments for experimental investigation of problems in fundamental and applied physics [183].

The first experiments on testing the rotational sensitivity of atomic interferometers were carried out by Riehle et al. [182] using optical Ramsey spectroscopy with calcium atomic beams. By rotating their setup at various angular velocities Ω and recording the edge shift of the Ramsey grating, the authors of [182] were the first to demonstrate the high resolution of atomic beam wave packet interferometry, or the interference of matter waves.

In 1997, two other research groups [184, 185] simultaneously published results on the detection of rotational effects by atomic interferometers. Each of these studies used its own method for realizing the interference of material waves. In [184], a beam of sodium atoms (with a longitudinal speed of ≈ 1030 m s^{-1}) was passed through three nanostructured gratings (period 200 nm, spacing 0.66 m), which caused splitting, reflection, and recombination of atomic wave packets. By setting and controlling the rotation of the setup, the authors measured the slow rotation speed of the same order of magnitude as Earth's rotation speed ($\Omega_{\rm E} \approx 73$ μrad s^{-1}), with a short-term sensitivity of about 3×10^{-6} Hz$^{1/2}$. Agreement with the theory at a 1% level was shown in a relatively wide range of $\pm 2\Omega_{\rm E}$, which corresponds to a tenfold increase in sensitivity compared to the first measurements [182].

In [185], a scheme for constructing an atomic interferometer was implemented that subsequently became the most common in such experiments. To change the state of cesium atoms (with a longitudinal speed of ≈ 290 m s^{-1}), three pairs of counter-propagating laser pulses with a judiciously selected duration were used (so-called Raman pulses $\pi/2$; π; $\pi/2$, with their duration marked by the phase oscillations of a two-level system). Two-photon excitation of transitions between long-lived states of the hyperfine splitting of the $6S_{1/2}$ level ($F = 3 \to F = 4$) was used to increase the effective momentum k transferred to the atoms.

By measuring the number of atoms that are in two states at the output of the interferometer, it is possible to construct interference patterns, which depend on the rotation speed of the interferometer. In [185], a short-term rotation sensitivity of 2×10^{-8} rad s^{-1} Hz$^{-1/2}$ was obtained.

The progress achieved to date in the technique of controlling the amplitude, wavelength, linewidth, and phase of waves emitted by lasers allows this scheme to be accepted, whenever its design does not involve moving parts, as a standard model for an atomic interferometer and to be used to explain the physics of the relevant processes.

In the case of Raman transitions, two long-lived ground states are typically used. Two laser beams with frequencies ω_1 and ω_2 are tuned, such that their difference $\Delta\omega$ corresponds to the transition between two hyperfine states, $|1\rangle$ and $|2\rangle$. When the beams propagate in the opposite direction (i.e., with the wave vectors $k_2 \approx -k_1$), momentum of the order of $2\hbar k_1$ is transferred to the atom. A sequence of short 'Raman' signals with durations of $\pi/2$; π; $\pi/2$ can be used to split the monostate of atoms into a superposition of $|1, p\rangle$ and $|2, p + \hbar k_{\rm eff}\rangle$, where $k_{\rm eff} = k_1 - k_2$, to exchange the atoms of this superposition, to recombine and split them again, and so on.

Figure 22 shows the most typical configuration of an atomic interferometer for detecting rotations [185]. A cloud of cooled atoms during its motion was irradiated sequentially by three Raman pulsed signals separated in time by an interval T. (The configuration of trajectories due to different velocities of atoms in different states is similar to that in the optical Mach–Zehnder interferometer.) At the output of the interferometer, the number of atoms N_1 and N_2 in the respective states $|1, p\rangle$ and $|2, p + \hbar k_{\rm eff}\rangle$ is recorded. The phase shift $\Phi_{\rm tot}$ between wave packets is related to the populations of N_1 and N_2 levels $|1\rangle$ and $|2\rangle$ as

$$\frac{N_2}{N_1 + N_2} = \frac{1 - \cos\Phi_{\rm tot}}{2} \,. \tag{8.1}$$

The total phase shift in the interferometer is expressed as

$$\Phi_{\rm tot} = (\varphi_1 - \varphi_2^{\rm A}) - (\varphi_2^{\rm B} - \varphi_3) \,, \tag{8.2}$$

where individual phases φ_i correspond to the ith Raman light pulse: $\varphi_i = k_{\rm eff} r(t_i) + \varphi_{\rm L}$. Here, $r(t_i)$ is the position of the center of mass of the wave packet, $\varphi_{\rm L}$ is the difference between the phases of two Raman lasers, and t_i is the time of the ith

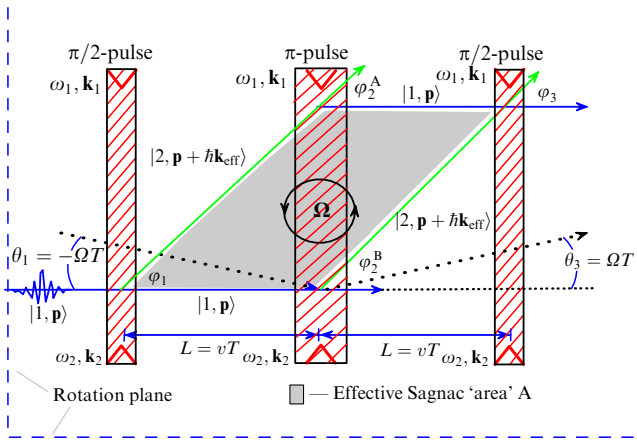

Figure 22. (Color online.) Cold-atom Sagnac interferometer. Schematic diagram of Sagnac interferometer on 'matter waves' using two-photon excitation by Raman pulses. Cooled cloud of atoms in the ϕ state with center-of-mass velocity $\mathbf{v} = \mathbf{p}/m$ is exposed to a sequence of Raman laser pulses that rotate relative to atomic trajectory with constant angular velocity Ω.

pulse. The indices A and B at φ_2 indicate the upper and lower paths (tracks) of the interferometer, as shown in Fig. 22.

In general, two types of interferometric signals due to inertial effects can be detected: a variation in the absolute velocity (i.e., linear acceleration) and a variation in the velocity vector (i.e., rotation). To measure linear accelerations, the sensitivity axis of the interferometer is directed along the propagation axis of laser beams. When registering rotations, the interferometer is sensitive to rotations about the axis perpendicular to the plane in which the atomic trajectories lie. The calculation of interferometer phase shifts in a noninertial (accelerating or rotating) reference frame is described in detail, e.g., in [178, 186–189].

A simplified estimate of the phase shift for an atomic interferometer in a reference frame rotating at a constant speed can be obtained as follows [190]. Let the Raman beams (lasers) rotate with a speed Ω in the reference frame associated with the atom (see Fig. 22). At $t = 0$, the orientation of the Raman beams is rotated through the angle $\theta_1 = -\Omega T$. Under the condition $|\theta|_1 \ll 1$, the phase shift is $\varphi_1 = k_{\mathrm{eff}}\theta_1 L$. At $t = T$, the Raman beam is perpendicular to the trajectory of the atom, and therefore the phase shift due to the rotation is zero. It can be shown that $\varphi_2^{\mathrm{A}} = -\varphi_2^{\mathrm{B}}$ in the center-of-mass system. Similarly, at $t = 2T$, the phase is $\varphi_3 = -k_{\mathrm{eff}}\theta_3 L$, where $\theta_3 = \Omega T$. Using the relation of Φ_{tot} to φ_i, it is easy to show that the total phase shift of the interferometer due to rotation is $\Phi_{\mathrm{rot}} = k_{\mathrm{eff}}(\theta_1 + \theta_3)L = -2k_{\mathrm{eff}}v\Omega T^2$, where v is the speed of atoms at the entrance to the interferometer. A more general form of this expression in the case where the rotation vector is not necessarily perpendicular to the interferometer plane was given in [186, 187]:

$$\Phi_{\mathrm{rot}} = -2(\mathbf{k}_{\mathrm{eff}} \times \mathbf{v})\,\mathbf{\Omega}T^2\,. \tag{8.3}$$

It follows that the rotation-induced phase shift depends linearly on v and Ω and quadratically on T (or L). Therefore, the sensitivity to rotation of an interferometer based on matter waves depends on the scale of the encompassed area, just as in the optical Sagnac interferometer. Indeed, Eqn (8.3) can be rewritten so as to explicitly isolate this 'area' dependence by defining the area vector $\mathbf{A} = (\hbar\mathbf{k}_{\mathrm{eff}}/M)T \times \mathbf{v}\,T$. Then, $\Phi_{\mathrm{rot}} = 2M\mathbf{A}\mathbf{\Omega}/\hbar$, which is equivalent to the Sagnac phase given in (2.4).

Formula (8.3) immediately suggests two ways of increasing the sensitivity by increasing the effective Sagnac area: to increase either the speed of atoms v or the probing (response) time interval T between Raman pulses. Both approaches have been implemented in experimental studies [191, 192]. In [191], a high initial speed of cold atoms was chosen. In addition, an original technique was used: two fluxes of atoms moved toward each other. In that case, in the interference patterns of two counter-propagating groups of atoms, one can filter out (separate) parasitic phase shifts arising, for example, due to acceleration under the action of gravity or mechanical vibrations of the installation. The following rotation accuracy has been achieved: 6×10^{-10} rad s^{-1} Hz$^{-1/2}$ [191] for the integration time of ~ 1 s and 8×10^{-12} rad s^{-1} [192] for 5 h of measurement accumulation. Experiments in which time T of the order of 100 ms was used are described in [193, 194], where the rotation was detected with an accuracy of 2.4×10^{-7} rad s^{-1} Hz$^{-1/2}$ for 1 s averaging and 1×10^{-8} rad s^{-1} for 1000 s averaging. Further improvements in the design scheme proposed in [195] allowed increasing the effective area to 11 cm^2 with a total interference cycle time $2T = 800$ ms.

Returning to the key idea of using the interference of matter waves in ring gyroscopes instead of optical-range EM waves, we can note the following. There is an obvious difference (even if only a formal one): in an atomic interferometer, atoms pass only half the perimeter of the area A. Perhaps, in the case of an atomic interferometer, it is not entirely correct to speak of the effective area. A strictly quantum mechanical description of the interferometer must be used, in which spatial localization of objects is no longer defined quite the same. From this standpoint, there may be no direct analogy between optical and atomic Sagnac gyroscopes.

The phase shift ratio for an atomic and optical interferometer was estimated in [196] as

$$\frac{\Delta\Phi_{\mathrm{at}}}{\Delta\Phi_{\mathrm{opt}}} = \frac{1}{2}\,\frac{mc^2}{h\nu}\,\frac{\mathbf{A}\mathbf{\Omega}}{\mathbf{S}\mathbf{\Omega}}\,. \tag{8.4}$$

This is the source of the emphasis (made in a number of papers) on the gain in sensitivity, because the ratio $mc^2/(h\nu)$ for ^{4}He atoms, Cs atoms, and the C_{60} molecule with $\lambda = 0.63$ μm is, respectively, 2×10^9, 6×10^{10}, and 3×10^{11} [196], demonstrating an apparent huge increase in efficiency per unit area of the interferometer. Formula (8.4), however, gives only an estimate of the conversion factor of the device, but not the signal-to-noise ratio. Nevertheless, this fact theoretically allows considering cold-atom SG installations (even those based on atomic chips) [197] of a much smaller size compared to optical geodetic interferometers of the same sensitivity.

We also note that, despite the successful practical implementation of atomic SGs, rigorous calculations of the phase shift based on exact solutions of the Schrödinger equations are not yet known. In [187], as in most other studies, the expression for the phase difference was obtained approximately in the first order of the expansion in the parameter $\Omega R/c$. The last known theoretical studies [196] already deal with attempts to take higher orders in $\Omega R/c$ into account. Perhaps this would lead to the discovery of new useful properties of atomic SGs.

To conclude this section, it is worth mentioning that a brief review of Sagnac rotation sensors based on other macroscopic manifestations of wave packet interference, including consideration of quantum effects in superfluid helium, can be found in [197, 198].

9. New concept of angle measurements

Ring lasers began to be used in the metrology of angle measurements in the late 1960s. A French patent [199] can probably be considered the first work in that field. The main idea of a dynamical laser goniometer (DLG) is to use the interference pattern from two counter-propagating waves in the laser ring as an ultrafine angular scale: a limb that divides the full angle 2π into $N_{2\pi} = 2P/\lambda$ intervals. It can be shown using formula (1.1) for the Sagnac splitting frequency δf_{Sagn} that this quantity corresponds to the number of periods (beats) of δf_{Sagn} during one full rotation of the gyrolaser platform (table). In the experiment, the number $N_{2\pi}$ is measured by a counter of pulses (interference fringes) within a fixed observation interval. For a ring laser with parameters $R \approx 0.5$ m and $\lambda \approx 0.5$ μm, the number of limb marks is of the order of $10^6 - 10^7$ (and can be increased by using the interpolation technique [200, 201]). This explains the high resolution of the DLG. The division value of one fringe is 0.1 arc seconds.

In general terms, the structure of a DLG can be represented as a vertical cylindrical rotor with a table mounted on it, which is a horizontal platform (round or square) carrying a ring laser whose output is a harmonic radio signal at the frequency δf_{Sagn} (Fig. 23). The rotor can also carry additional parallel platforms for other types of angle transformers, angular measures under study, and so on (Fig. 24) [200, 201].

The actual number of fringes observed in the time $t_1 - t_0$ during which the table rotates through the angle φ is $N_\varphi = [K/(2\pi)]\varphi$. The number of fringes observed during the period $T = 2\pi/\Omega$ of one full revolution of the table is $N_{2\pi} = K$, where $K = [4A/(\lambda P)]\cos\theta$ (see (1.1)) is the angle conversion factor, a constant characteristic of a given instrument at a given location. The conversion factor K can be accurately determined each time a measurement is made, so as to ensure absolute autocalibration of the apparatus without involving any a priori information about its exact geometry and environment. The measured angle of rotation is expressed by the simple formula

$$\varphi = 2\pi \frac{N_\varphi}{N_{2\pi}} . \tag{9.1}$$

The option of absolute autocalibration is the second important property of this device and the technique itself.

The described scheme for measuring the rotor rotation angle φ assumes the presence of another node, the so-called null indicator (NI), to indicate the reference directions that specify the angle values. This is either an accurate chronometer that fixes the moments of the observation interval t_0 and t_1 or a photoelectric detector that registers strokes on the perimeter of the platform. In any case, the NI is located in the immovable part of the DLG, for example, on its stator (Fig. 25). The error in measuring the angle φ, Eqn (9.1), is related to the error in counting the number of fringes N_φ. Two components of the error are obvious: (1) fluctuations in the frequency of the ring laser output signal $\delta\omega(t)$, and (2) the error in fixing the reference interval (moments t_0 and t_φ). The first is determined by the instability of the rotation of the

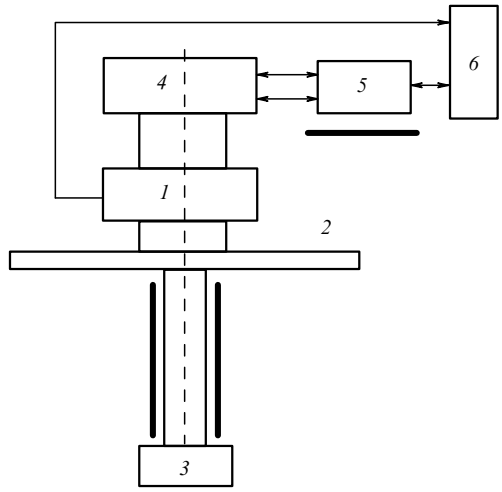

Figure 23. Schematic diagram of a dynamical laser goniometer: *1* — ring laser, *2* — goniometer rotor, *3* — drive, *4* — polyhedral prism, *5* — null indicator, *6* — interface.

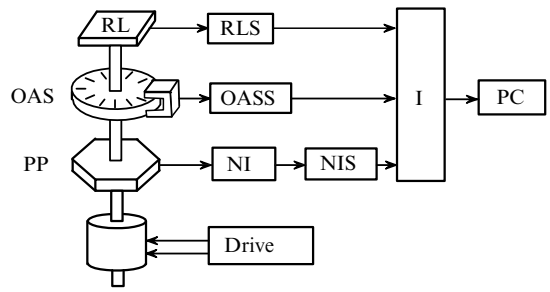

Figure 24. Diagram of DLG rotor with calibration platforms. OAS — optical angle sensor, PP — polyhedral prism, RLS — ring laser shaper, OASS — optical angle sensor shaper, NIS — null indicator shaper, I — interface, PC — personal computer.

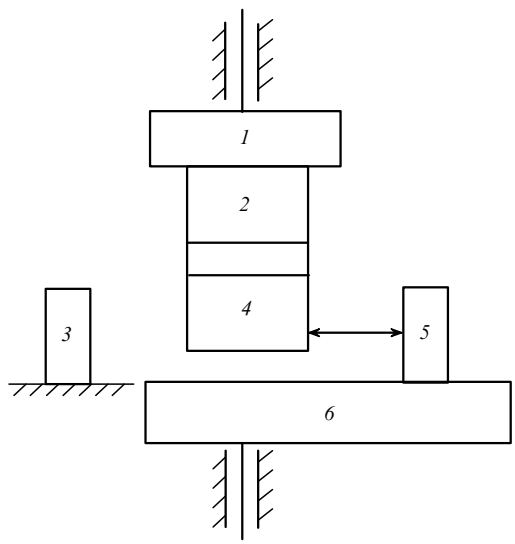

Figure 25. Setup for measuring the angular position of external objects: *1* — goniometer rotor, *2* — ring laser, *3* — reference mirror, *4* — null indicator, *5* — controlled mirror, *6* — measurement object.

goniometer rotor and fluctuations in the laser radiation frequency. The second, in addition to rotation instability, is also affected by the NI noise. Numerical evaluations require information about technological parameters. There are specific devices SG-1L and IUP-1L (developed by the Ulyanov St. Petersburg State Electrotechnical University LETI using a KM-11 ring laser manufactured by the Joint Stock Company Stelmakh Scientific Research Institute Polyus [200–202]). The correlation analysis of errors for these DLGs, carried out in [201], gives an estimate of the φ measurement error at the level of $\sigma_\varphi \leqslant 0.05''$. At the same time, the potential sensitivity (the minimum detectable angle) due only to the presence of quantum fluctuations of laser radiation is of the order of $\sigma_\varphi \sim 0.001'$. This motivates research to reduce the error of the existing DLG prototypes. Currently, work is in progress at the National Institute for Metrological Research INRIM (Istituto Nazionale di Ricerca Metrologica) (Turin, Italy) in collaboration with INFN. The goal of the project is to create a portable goniometer with an angular accuracy of $0.002''$ (or 10 nrad) [203].

In addition to registering proper angular rotation, the DLG is able to control the angular motions of external objects. For example, the so-called inverted laser goniometer allows measuring the angular position of objects in order to apply angular calibration strokes to them. In such a scheme, the goniometer rotor is arranged coaxially with the turntable on which the object is placed. The NI is now fixed on the goniometer rotor. A reference mirror is installed outside the goniometer on a fixed base, and a control mirror is attached to the object (see Fig. 25). Rotating together with the rotor, the NI generates reference pulses at the instants when its optical axis (beam) coincides with the normals to both mirrors.

Furthermore, it is possible to measure the angular position of objects located at a considerable distance from the DLG, which allows this tool to play the role of a precision autocollimator or theodolite. In this capacity, the DLG axis carries a platform with a polyhedral prism (PP), by means of which the beam of a fixed NI (on an external base) is scanned while running through a control mirror glued to the object being measured. The NI generates reference pulses when the light beam simultaneously hits the control mirror and the reference mirror (in this setup, installed on the DLG base). The frequency of measuring the angular position of an object is the rotation velocity times the number of PP faces: $f = n\Omega/(2\pi)$. The setups discussed here are considered in detail in [204, 205].

We remark on the fundamental systematic errors in angular measurements involving ring lasers. One of the most significant sources of systematic error in ring lasers is the influence of Earth's external magnetic field. A ring laser has a certain axis of sensitivity to a magnetic field, which lies in the plane of its cavity [206]. Under rotation, this axis changes its orientation relative to the magnetic field lines, which leads to a systematic error (at a constant magnetic field) in the first harmonic of the rotation frequency. In principle, this error component can be taken into account and compensated algorithmically. However, Earth's rotation itself creates an addition to the frequency of the output signal of the ring laser. Due to the instability of the rotation speed, this addition causes systematic distortions of the angular scale of the ring laser. The use of phase–time correction algorithms [207] allows practically eliminating the corresponding systematic error and the shift of zero of the ring laser. A description of the metrological properties of DLGs clearly emphasizes the important role that such tools can play in mechanical engineering, in industries requiring increased angular control, in metrology for the manufacture of solid angular measures, and so on. At the same time, we note the applications of DLGs to fundamental research, in particular, in crystallography in preparing specific crystal sections. Applications to astronomy and geodesy should be noted in view of the need to control and calibrate (to the level of several nanoradians) the complex angular motion of multi-axis structures such as large antenna systems and optical telescopes.

10. Conclusion

We have tried to draw the attention of researchers involved in experimental studies in the fields of astronomy, gravity, geophysics, laser physics, and elementary particle physics to a specific and already significantly developed field of research activity associated with the presence of a surprisingly versatile measuring instrument — the gravity-inertial sensor, which we refer to as a Sagnac gyroscope. Indeed, the list of possible applications of such an instrument, already illustrated by the title of this review, testifies to the broad possibilities of the Sagnac gyroscope. At the same time, each specific application has its own characteristics and requires a thorough analysis. Below, we formulate a brief summary of the applications discussed in this review, but first we give information about the related material available in the literature.

In 2014, the journal *Comptes Rendus Physique*, part of a group of publications by IOP Publishing (Elsevier), dedicated a separate issue 10 [208] to the 100th anniversary of the publication in the same journal of the original article by Georges Sagnac [1] describing the effect that later received his name. The jubilee issue contained invited papers from research groups involved in the development and applications to fundamental and applied physics at various facilities based on the Sagnac effect. The breadth of coverage of the related physical problems somewhat exceeds the range of topics covered in this review. The refrain from article to article concerns the fact that Sagnac himself hardly surmised the true role and fate of his discovery, considering it one of the manifestations of SR. The same issue contains a review and biographical article on the scientific heritage of this scientist [209].

We briefly summarize the main conclusions that, in our opinion, follow from this review.

It can be stated that, in practice, the minimal relative variations in the angular velocity of Earth's rotation recorded by large SGs remain at the level of 10^{-8} in measurements at times of the order of a day, which is an order of magnitude less than the design sensitivity expected from these installations. Although methods for increasing the sensitivity have been indicated, no silver bullet strategy is known that would guarantee success, at least for optical range rings.

However, the achieved resolution of large-scale installations is already sufficient to track short geodynamical perturbations of Earth's interior and monitor natural disasters using circulating surface seismic waves. Also unique will be direct information about the excitation of global toroidal modes, which is inaccessible to other geophysical instruments.

The desire to register and more accurately measure the relativistic correction to the gravitational field of rotating

Earth (the LT effect), of course, has a heuristic and original character as a measurement from the inside of a gravitating object. But the implementation of this program is very challenging. As a rigorous analysis has shown, a long-term collection of data over an interval of several years will be required. Systematic filtering requires a comparison of measurement results at several remote sites (BNO is one possibility), but this has yet to be arranged.

In DM search experiments, ring lasers have not yet had their last say. As our analysis shows, ring lasers can allow advances by more than an order of magnitude in estimating both the axion–photon coupling constant and the mass of ALPs. However, this involves the use of rings with high luminous power, up to 100 W, a technique that has yet to be mastered.

As regards the use of SG rings for EP tests related to Lorentz invariance, it should be expected to be continued, because only rotational designs provide locality of the kinematic setup. In addition, LI tests related to SM particles are associated with the measurement of many multiparameters (entire tables), which is laborious and time consuming.

The analysis of the current state of GW experiments suggests that, with a high probability, new-generation gravitational antennas will have the topology of combined Sagnac–Michelson interferometers, mainly because this is currently the only configuration that allows overcoming quantum sensitivity limitations, regardless of the success of the technique of producing squeezed states of optical pumping and of a vacuum.

As regards the transition from optical laser rings of SGs to quantum interferometers based on cold atoms, despite the obvious promise of such a step, its fundamental and practical possibility remains vague. It is still not entirely clear whether 'atomic rotation sensors' are in fact ring SGs. There is a lack of clarity regarding the need for and acceptability of such large installations.

On the contrary, there is no doubt about the usefulness of the SG technique in precision angular measurements, which have already been developed and tested in sufficient detail. However, a 'journal for proposals' on the use of this unique property of SGs as goniometers to solve the fundamental problems of astrophysics, geophysics, and gravity remains largely unwritten.

The same can be seen in relation to the advantages, repeatedly emphasized in this review, that geodetic SGs have as local compasses of Earth's orientation relative to the celestial compass of VLBI systems. The possibility of such two-way control by measurement should stimulate the design of projects on a planetary, galactic, and even larger scale — for as long as this niche remains free.

To conclude, we express our sincere gratitude to the colleagues whose advice and direct assistance was instrumental in preparing this multidisciplinary review. They are, first of all, colleagues from the Sternberg State Astronomical Institute and the Faculty of Physics of Moscow State University: A M Cherepashchuk, K A Postnov, V E Zharov, and F Ya Khalili; from the Institute of Laser Physics, SB RAS: S N Bagaev and M N Skvortsov; from INR RAS: S V Troitsky and P S Satunin; from the Hydrometeorological Center: N S Sidorenko; from BNO RAS: V B Petkov, V V Kuzminov, R V Novoseltseva, and A N Gangapshev; from the Schmidt Institute of Physics of the Earth, RAS: A B Manukin and V I Osika; from JSC Stelmakh Research Institute Polyus: V V Azarova and Yu D Golyaev; as well as our foreign partners from INFN Pisa: A Di Vergilio and N Beverini. This work was supported by the Russian Foundation for Basic Research grant MK 19-29-11010.

References

1. Sagniac G *C.R. Acad. Sci. Paris* **157** 708 (1913)
2. Sagniac G *J. Phys. Theor. Appl.* **4** 177 (1914)
3. Stedman G E *Rep. Prog. Phys.* **60** 615 (1977)
4. Michelson A A, Gale H G *Astrophys. J.* **61** 140 (1925)
5. Schreiber K U et al. *C.R. Phys.* **15** 859 (2014)
6. Rowe C H et al. *Appl. Opt.* **38** 2516 (1999)
7. Bosi F et al. *Phys. Rev. D* **84** 122002 (2011)
8. Hughes V W, in *Gravitation and Relativity* (Eds H-Y Chiu, W F Hoffmann) (New York: W.A. Benjamin, 1964) Ch. 6; Translated into Russian: in *Gravitatsiya i Otnositel'nost'* (Eds H-Y Chiu, W F Hoffmann) (Moscow: Mir, 1965) Ch. 6; Dicke R H, in *Gravitation and Relativity* (Eds H-Y Chiu, W F Hoffmann) (New York: W.A. Benjamin, 1964) Ch. 7; Translated into Russian: in *Gravitatsiya i Otnositel'nost'* (Eds H-Y Chiu, W F Hoffmann) (Moscow: Mir, 1965) Ch. 7; Wheeler J A, in *Gravitation and Relativity* (Eds H-Y Chiu, W F Hoffmann) (New York: W.A. Benjamin, 1964) Ch. 15; Translated into Russian: in *Gravitatsiya i Otnositel'nost'* (Eds H-Y Chiu, W F Hoffmann) (Moscow: Mir, 1965) Ch. 15
9. Cooper L, Stedman G E *Phys. Lett. B* **357** 464 (1995)
10. Raffelt G G *J. Phys. A* **40** 6607 (2007)
11. Logunov A A, Chugreev Yu V *Sov. Phys. Usp.* **31** 861 (1988); *Usp. Fiz. Nauk* **156** 137 (1988)
12. Malykin G B *Phys. Usp.* **43** 1229 (2000); *Usp. Fiz. Nauk* **170** 1325 (2000)
13. Gustavson T L, Bouyer P, Kasevich M A *Phys. Rev. Lett.* **78** 2046 (1997)
14. Einstein A *Ann. Physik* **17** 891 (1905); Translated into Russian: *Sobranie Sochinenii* (Collected Works) Vol. 1 (Moscow: Nauka, 1965) p. 7
15. Misner C W, Thorne K S, Wheeler J A *Gravitation* (San Francisco, CA: W.H. Freeman and Co., 1973); Translated into Russian: *Gravitatsiya* Vol. 1 (Moscow: Mir, 1977) p. 207
16. Einstein A *Sitzungsber. preuß. Akad. Wiss.* **2** 1030 (1914); Translated into Russian: *Sobranie Sochinenii* (Collected Works) Vol. 1 (Moscow: Nauka, 1965) p. 326
17. Logunov A *Lectures in Relativity and Gravitation: a Modern Look* (Oxford: Pergamon Press, 1990); Translated from Russian: *Lektsii po Teorii Otnositel'nosti i Gravitatsii. Sovremennyi Analiz Problemy* (Moscow: Nauka, 1987)
18. Landau L D, Lifshitz E M *The Classical Theory of Fields* (Oxford: Pergamon Press, 1971); Translated from Russian: *Teoriya Polya* 7th ed. (Moscow: Nauka, 1988)
19. Belenov E M, Markin E P *JETP Lett.* **7** 381 (1968); *Pis'ma Zh. Eksp. Teor. Fiz.* **7** 497 (1968)
20. Fateev V F *Opt. Spectrosc.* **54** 412 (1983); *Opt. Spektrosk.* **54** 697 (1983)
21. Lense J, Thirring H *Phys. Z.* **19** 156 (1918)
22. Hönl H *Naturwissenschaften Reihe* **15** 1 (1966); Translated into Russian: in *Einsteinovskii Sbornik* (Einstein Collection) (Eds I E Tamm, G I Naan) (Moscow: Nauka, 1968) p. 258
23. Rothacher M et al. *J. Geophys. Res.* **106** 13711 (2001)
24. Macek W M, Davis D T M (Jr.) *Appl. Phys. Lett.* **2** 67 (1963)
25. Di Virgilio A et al. *Class. Quantum Gravity* **27** 084033 (2010)
26. Belfi J et al. *IEEE Trans.* **57** 3 (2010)
27. Schreiber K U, Wells J-P R *Rev. Sci. Instrum.* **84** 041101 (2013)
28. Rowe C H et al. *Appl. Opt.* **38** 2516 (1999)
29. Dunn R W et al. *Appl. Opt.* **41** 1685 (2002)
30. Hurst R B et al. *J. Appl. Phys.* **105** 113115 (2009)
31. Pritsch B et al. *Appl. Phys. Lett.* **91** 061115 (2007)
32. Sidorenkov N S *The Interaction between Earth's Rotation and Geophysical Processes* (Weinheim: Wiley-VCH, 2009)
33. Sidorenkov N S *Astron. Astrophys. Trans.* **24** 425 (2005)
34. Schreiber K U et al. *Phys. Rev. Lett.* **107** 173904 (2011)
35. Igel H et al. *Geophys. Res. Lett. L* **32** 08309 (2005)
36. Igel H et al. *Geophys. J. Int.* **168** 182 (2007)

37. Cochard A et al., in *Earthquake Source Asymmetry, Structural Media and Rotational Effects* (Eds R Teisseyre, E Majewski, M Takeo) (Berlin: Springer, 2006) p. 391, https://doi.org/10.1007/3-540-31337-0
38. Fichtner A, Igel H *Bull. Seismol. Soc. Am.* **99** 1302 (2009)
39. Bernauer M, Fichtner A, Igel H *Geophysics* **74** (6) WCD41 (2009)
40. Igel H et al. *Geophys. Res. Lett.* **38** L21303 (2011)
41. Widmer-Schnidrig R, Zürn W *Bull. Seismol. Soc. Am.* **99** 1199 (2009)
42. Nader M F et al. *J. Seismol.* **16** 745 (2012)
43. Nader M F et al. *Geophys. J. Int.* **201** 1482 (2015)
44. Aki K, Richards P G *Quantitative Seismology* 2nd ed. (Sausalito, CA: Univ. Science Books, 2002)
45. Schreiber U et al., in *Proc. of the 11th Intern. Conf. on Integrated Navigation Systems, St. Petersburg, 2004* (St. Petersburg: TsNII Elektropribor, 2004)
46. Pancha A et al. *Geophys. Res. Lett.* **27** 3553 (2000)
47. Plag H-P, Pearlman M (Eds) *Global Geodetic Observing System* (Berlin: Springer, 2009) https://doi.org/10.1007/978-3-642-02687-4
48. Thirring H *Phys. Z.* **19** 204 (1918)
49. Schiff L I *Proc. Natl. Acad. Sci. USA* **46** 871 (1960)
50. Everitt C W F et al. *Phys. Rev. Lett.* **106** 2211014 (2011); arXiv:1105.3456
51. Ciufolini I, Pavlis E C *Nature* **431** 958 (2004)
52. Missions - LAGEOS 1&2. NASA Science, 4 May 1976, http://science.nasa.gov
53. Fisher A *Popular Sci.* **209** (1) 10 (1977)
54. Van Patten R A, Everitt C W F *Phys. Rev. Lett.* **36** 629 (1976)
55. Ciufolini I et al. *Class. Quantum Gravity* **14** 2701 (1997)
56. Ciufolini I et al. *Science* **279** 2100 (1998)
57. Ciufolini I et al. *Eur. Phys. J. Plus* **126** 72 (2011)
58. Paolozzi A, Ciufolini I *Acta Astronaut.* **91** 313 (2013); arXiv:1305.6823
59. Will C M *Living Rev. Relativ.* **17** 4 (2014)
60. Burgay M et al. *Nature* **426** 531 (2003)
61. Ciufolini I, Wheeler J A *Gravitation and Inertia* (Princeton, NJ: Princeton Univ. Press, 1995)
62. Raine D, Thomas E *Black Holes: An Introduction* (Hackensack, NJ: World Scientific, 2010)
63. Stedman G E, Schreiber K U, Bilger H R *Class. Quantum Gravity* **20** 2527 (2003)
64. Di Virgilio A et al. *Int. J. Mod. Phys. D* **19** 2331 (2010)
65. Di Virgilio A et al. *C. R. Phys.* **15** 866 (2014)
66. Beverini N et al. *Laser Phys.* **24** 074005 (2014)
67. GINGER: Gyroscopes in General Relativity, http://web2.infn.it/GINGER/index.php/it/
68. Santagata R et al. *Class. Quantum Gravity* **32** 055013 (2015)
69. NEWSLETTER 35, May 2017, p. 10. INFN, https://home.infn.it/newsletter-eu/pdf/NEWSLETTER_INFN_35_inglese_10.pdf
70. Peccei R D, Quinn H R *Phys. Rev. Lett.* **38** 1440 (1977)
71. Peccei R D, Quinn H R *Phys. Rev. D* **16** 1791 (1977)
72. Weinberg S *Phys. Rev. Lett.* **40** 223 (1978)
73. Wilczek F *Phys. Rev. Lett.* **40** 279 (1978)
74. Preskill J, Wise M B, Wilczek F *Phys. Lett. B* **120** 127 (1983)
75. Dine M, Fischler W *Phys. Lett. B* **120** 137 (1983)
76. Abbott L F, Sikivie P *Phys. Lett. B* **120** 133 (1983)
77. Davis R L *Phys. Lett. B* **180** 225 (1986)
78. Lyth D H *Phys. Lett. B* **275** 279 (1992)
79. Svrcek P, Witten E *J. High Energy Phys.* (06) 051 (2006); hep-th/0605206
80. Arvanitaki A et al. *Phys. Rev. D* **81** 123530 (2010); arXiv:0905.4720
81. Sikivie P *Phys. Rev. Lett.* **51** 1415 (1983)
82. Sikivie P *Phys. Rev. D* **32** 2988 (1985)
83. DePanfilis S et al. *Phys. Rev. Lett.* **59** 839 (1987)
84. Wuensch W et al. *Phys. Rev. D* **40** 3153 (1989)
85. Lazarus D M et al. *Phys. Rev. Lett.* **69** 2333 (1992)
86. Semertzidis Y et al. *Phys. Rev. Lett.* **64** 2988 (1990)
87. Hagmann C et al. *Phys. Rev. D* **42** 1297 (1990)
88. Asztalos S J et al. *Phys. Rev. D* **64** 092003 (2001); The Axion Dark Matter eXperiment. Department of Physics, Univ. of Washington, http://depts.washington.edu/admx/index.shtml
89. Carrack new. Research Center for Low Temperature and Materials Sciences, Kyoto Univ., http://www.ltm.kyoto-u.ac.jp/
90. Moriyama S et al. *Phys. Lett. B* **434** 147 (1998); hep-ex/9805026
91. Anastassopoulos V et al. (CAST Collab.) *Nat. Phys.* **13** 584 (2017); arXiv:1705.02290
92. ADMX, http://www-pat.llnl.gov/N_Div/Axion/axion.html
93. Duffy L D et al. *Phys. Rev. D* **74** 012006 (2006)
94. http://cast.web.cern.ch/CAST/
95. Iguaz F J (for the CAST Collab.), arXiv:1110.2116
96. Spector A (for the ALPS Collab.), arXiv:1906.09011
97. Tran Tan H B et al. *Phys. Dark Univ.* **24** 100272 (2019); arXiv:1803.09388
98. Jackson Kimball D F et al., in *Microwave Cavities and Detectors for Axion Research. Proc. of the 3rd Intern. Workshop* (Springer Proc. in Physics, Vol. 245, Eds G Carosi, G Rybka) (Cham: Springer, 2020) p. 105, https://doi.org/10.1007/978-3-030-43761-9_13; arXiv:1711.08999
99. Ehret K et al. *Phys. Lett. B* **689** 149 (2010); arXiv:1004.1313
100. Betz M et al. *Phys. Rev. D* **88** 075014 (2013); arXiv:1310.8098
101. Bogorad Z et al. *Phys. Rev. Lett.* **123** 021801 (2019); arXiv:1902.01418
102. Gao C, Harnik R, arXiv:2011.01350
103. Salnikov D et al. *J. High Energ. Phys.* **2021** 143 (2021); arXiv:2011.12871
104. Irastorza I G, Redondo J *Prog. Part. Nucl. Phys.* **102** 89 (2018); arXiv:1801.08127
105. Troitsky S *Phys. Rev. D* **93** 045014 (2016); arXiv:1507.08640
106. Kuster M et al. *Axions: Theory, Cosmology, and Experimental Searches* (Lecture Notes in Physics, Vol. 741, Eds M Kuster, G Raffelt, B Beltrán) (Berlin: Springer-Verlag, 2008) https://doi.org/10.1007/978-3-540-73518-2
107. Kobychev V, Popov S, Troitskii Variant No. 4 (173) (2015)
108. Sparnaay M J *Nature* **180** 334 (1957)
109. Bordag M et al. *Advances in the Casimir Effect* (Oxford: Oxford Univ. Press, 2009)
110. Mostepanenko V M, Trunov N N *Sov. Phys. Usp.* **31** 965 (1988); *Usp. Fiz. Nauk* **156** 385 (1988)
111. Barash Yu S, Ginzburg V L *Sov. Phys. Usp.* **18** 305 (1975); *Usp. Fiz. Nauk* **116** 5 (1975)
112. Masuda M et al. *Phys. Rev. Lett.* **102** 171101 (2009)
113. Fouché M, Battesti R, Rizzo C *Phys. Rev. D* **93** 093020 (2016); arXiv:1605.04102
114. Pugnat P et al. *Czech. J. Phys.* **55** A389 (2005)
115. Zavattini E et al. *Phys. Rev. Lett.* **96** 110406 (2006); hep-ex/0507107
116. Zavattini E et al. *Phys. Rev. D* **77** 032006 (2008); arXiv:0706.3419
117. Della Valle F et al. *Phys. Rev. D* **90** 092003 (2014); arXiv:1406.6518
118. Zavattini G et al. *Eur. Phys. J. C* **76** 294 (2016); arXiv:1601.03986
119. Della Valle F et al. *Eur. Phys. J. C* **76** 24 (2016); arXiv:1510.08052
120. Obata I, Fujita T, Michimura Y *Phys. Rev. Lett.* **121** 161301 (2018); arXiv:1805.11753
121. Drever R W P et al. *Appl. Phys. B* **31** 97 (1983)
122. Gavrilyuk Yu M et al. *JETP Lett.* **101** 664 (2015); *Pis'ma Zh. Eksp. Teor. Fiz.* **101** 739 (2015)
123. Gavriljuk Ju M et al. *Nucl. Instrum. Meth. Phys. Res. A* **729** 576 (2013)
124. Gavrilyuk Yu M et al. *JETP Lett.* **107** 589 (2018); *Pis'ma Zh. Eksp. Teor. Fiz.* **107** 617 (2018)
125. Nagashima Y *Elementary Particle Physics: Foundations of the Standard Model* Vol. 2 (Weinheim: Wiley-VCH, 2013)
126. Schwartz M D *Quantum Field Theory and the Standard Model* (New York: Cambridge Univ. Press, 2014)
127. Emel'yanov V M *Standartnaya Model' i ee Rasshireniya* (Standard Model and Its Extensions) (Moscow: Fizmatlit, 2007)
128. Kostelecký V A, Russell N *Rev. Mod. Phys.* **83** 11 (2011)
129. Kostelecký V A, Mewes M *Phys. Rev. D* **85** 096005 (2012); *Phys. Rev. D* **88** 096006 (2013)
130. Michimura Y et al. *Phys. Rev. Lett.* **110** 200401 (2013); arXiv:1307.5266
131. Wolf P et al. *Phys. Rev. D* **70** 051902 (2004)
132. Herrmann S et al. *Phys. Rev. Lett.* **95** 150401 (2005)
133. Eisele Ch, Nevsky A Yu, Schiller S *Phys. Rev. Lett.* **103** 090401 (2009)
134. Herrmann S et al. *Phys. Rev. D* **80** 105011 (2009)
135. Parker S R et al. *Phys. Rev. Lett.* **106** 180401 (2011)
136. Michimura Y et al. *Phys. Rev. D* **88** 111101 (2013); arXiv:1310.1952

137. Trimmer W S N et al. *Phys. Rev. D* **8** 3321 (1973)
138. Tobar M E et al. *Phys. Rev. D* **71** 025004 (2005)
139. Exirifard Q *Int. J. Mod. Phys. D* **23** 1450038 (2014); arXiv:1010.2057
140. Heansch T W, Couillaud B *Opt. Commun.* **35** 441 (1980)
141. Weiss R, Quarterly Progress Report, No. 105 (Cambridge, MA: Research Laboratory of Electronics, MIT, 1972) p. 54; NSF Proposal (1987)
142. Drever R W P, in *Gravitational Radiation. Summer School, Les Houches, France, 2–21 June 1982* (Eds N Deruelle, T Piran) (Amsterdam: North-Holland, 1983) p. 955
143. Sun K-X et al. *Phys. Rev. Lett.* **76** 3053 (1996)
144. Abbott B P et al. (LIGO Scientific Collab., Virgo Collab.) *Phys. Rev. Lett.* **116** 061102 (2016)
145. Abbott B P et al. (LIGO Scientific Collab., Virgo Collab.) *Phys. Rev. Lett.* **119** 141101 (2017)
146. Abbott B P et al. (LIGO Scientific Collab., Virgo Collab.) *Phys. Rev. Lett.* **119** 161101 (2017)
147. Mizuno J et al. *Opt. Commun.* **138** 383 (1997)
148. Lück H et al., 2007 Plans for E.T. (Einstein Telescope), A European 3rd generation gravitational wave observatory, presented at the AMALDI 7 conference, Sydney Einstein gravitational wave Telescope 2007 Design study proposal submitted to European Union. Framework 7, INFRA-2007-2.1-01, Design studies for research infrastructures in all S&T fields
149. Gustafson E et al., LIGO Document Number T990080-00-D, https://dcc.ligo.org/LIGO-T990080/public
150. Freise A et al. *Class. Quantum Gravity* **26** 085012 (2009); arXiv:0804.1036
151. Braginskii V B, Vorontsov Yu I *Sov. Phys. Usp.* **18** 644 (1975); *Usp. Fiz. Nauk* **114** 41 (1974);
152. Braginskii V B, Vorontsov Yu I, Khalili F Ya *Sov. Phys. JETP* **46** 705 (1977); *Zh. Eksp. Teor. Fiz.* **73** 1340 (1977)
153. Thorne K S et al. *Phys. Rev. Lett.* **40** 667 (1978)
154. Gusev A V, Rudenko V N *Sov. Phys. JETP* **49** 755 (1979); *Zh. Eksp. Teor. Fiz.* **76** 1488 (1979)
155. Grishanin B A, Stratonovich R L *Problems Information Transmission* **6** (3) 200 (1970); *Problemy Peredachi Inform.* **6** (3) 15 (1970)
156. Stratonovich R L *IEEE* **22** 303 (1974)
157. Dodonov V V, Man'ko V I, Rudenko V N *Sov. Phys. JETP* **51** 443 (1980); *Zh. Eksp. Teor. Fiz.* **78** 881 (1980)
158. Dodonov V V, Man'ko V I, Rudenko V N *Found. Phys.* **13** 607 (1983)
159. Caves C M *Phys. Rev. D* **23** 1693 (1981)
160. Kulagin V V, Rudenko V N *Nuovo Cimento C* **10** 601 (1987)
161. Kulagin V V, Rudenko V N *Sov. Phys. JETP* **67** 677 (1988); *Zh. Eksp. Teor. Fiz.* **94** (4) 51 (1988)
162. Bagaev S N et al. *Rev. Sci. Instrum.* **85** 065114 (2014)
163. Braginsky V B, Khalili F Ja *Phys. Lett. A* **147** 251 (1990)
164. Braginsky V B, Khalili F Ya *Quantum Measurement* (Cambridge: Cambridge Univ. Press, 1992)
165. Khalili F Ya, gr-qc/0211088
166. Chen Y *Phys. Rev. D* **67** 122004 (2003)
167. Danilishin S L *Phys. Rev. D* **69** 102003 (2004)
168. Meers B J *Phys. Rev. D* **38** 2317 (1988)
169. Adhikari R X *Rev. Mod. Phys.* **86** 121 (2014)
170. Voronchev N V, Danilishin Sh L, Khalili F Ya *Moscow Univ. Phys. Bull.* **69** 519 (2014); *Vestn. Mosk. Univ. Ser. 3 Fiz. Astron.* (6) 81 (2014)
171. Gräf C et al. *Class. Quantum Gravity* **31** 215009 (2014); arXiv:1405.2783
172. Danilishin S L, Khalili F Ya *Living Rev. Relativ.* **15** 5 (2012)
173. Gertsenshtein M E, Kobzev V V *Radiotekh. Elektron.* **19** 1330 (1974)
174. Dodonov V V, Man'ko V I, Rudenko V N *Sov. J. Quantum Electron.* **10** 1232 (1980); *Kvantovaya Elektron.* **7** 2124 (1980)
175. Abbott B et al. (LIGO Scientific Collab.) *New J. Phys.* **11** 073032 (2009)
176. Borde Ch J et al. *J. Physique Lett.* **44** 983 (1983)
177. Chebotayev V P et al. *J. Opt. Soc. Am. B* **2** 1791 (1985)
178. Clauser J F *Phys. B + C* **151** 262 (1988)
179. Kasevich M, Chu S *Phys. Rev. Lett.* **67** 181 (1991)
180. Carnal O, Mlynek J *Phys. Rev. Lett.* **66** 2689 (1991)
181. Keith D W et al. *Phys. Rev. Lett.* **66** 2693 (1991)
182. Riehle F et al. *Phys. Rev. Lett.* **67** 177 (1991)
183. Cronin A D, Schmiedmayer J, Pritchard D E *Rev. Mod. Phys.* **81** 1051 (2009)
184. Lenef A et al. *Phys. Rev. Lett.* **78** 760 (1997)
185. Gustavson T L, Bouyer P, Kasevich M A *Phys. Rev. Lett.* **78** 2046 (1997)
186. Storey P, Cohen-Tannoudji C *J. Phys. II France* **4** 1999 (1994)
187. Bordé Ch J *C. R. Acad. Sci. Phys.* **2** 509 (2001)
188. Bordé Ch J *Metrologia* **39** 435 (2002)
189. Antoine Ch, Bordé Ch J *Phys. Lett. A* **306** 277 (2003)
190. Barrett B et al. *C.R. Phys.* **15** 875 (2014)
191. Gustavson T L, Landragin A, Kasevich M A *Class. Quantum Gravity* **17** 2385 (2000)
192. Durfee D S, Shaham Y K, Kasevich M A *Phys. Rev. Lett.* **97** 240801 (2006)
193. Canuel B et al. *Phys. Rev. Lett.* **97** 010402 (2006)
194. Gauguet A et al. *Phys. Rev. A* **80** 063604 (2009)
195. Stockton J K, Takase K, Kasevich M A *Phys. Rev. Lett.* **107** 133001 (2011)
196. Krobka N I *Giroskop. Navig.* (3) 36 (2009)
197. Garrido Alzar C L *AVS Quantum Sci.* **1** 014702 (2019)
198. Sato Y *C.R. Phys.* **15** 898 (2014)
199. Catherin J M, Dessus B, French Patent 1511089 (granted 26.01.68)
200. Burnashev M N, Pavlov P A, Filatov Yu V *Quantum Electron.* **43** 2130 (2013); *Kvantovaya Elektron.* **43** 2130 (2013)
201. Burnashev M N et al. *Quantum Electron.* **30** 2141 (2000); *Kvantovaya Elektron.* **30** 2141 (2000)
202. Polyus Scientific Research Institute, https://niipolyus.ru/
203. Pisani M et al. *J. Phys. Conf. Ser.* **1065** 032009 (2018)
204. Filatov Yu V, Loukianov D P, Probst R *Metrologia* **34** 343 (1997)
205. Filatov Yu V, Loukianov D P, Pavlov P A, VDI Reports No. 1118 (1994) p. 123
206. Krivtsov E P, Filatov Yu V *Meas. Tech.* **32** 1140 (1989); *Izmer. Tekh.* (12) 11 (1989)
207. Pavlov P A *Meas. Tech.* **51** 22 (2008); *Izmer. Tekh.* (1) 17 (2008)
208. Gauguet A (Ed.) "The Sagnac effect: 100 years later" *C. R. Phys.* **15** (10) (2014)
209. Darrigol O *C.R. Phys.* **15** (10) 789 (2014)